Statistical mechanics of supercoiled DNA

J. F. Marko
Center for Studies in Physics and Biology, The Rockefeller University, 1230 York Avenue, New York, New York 10021-6399

E. D. Siggia
Laboratory of Atomic and Solid State Physics, Clark Hall, Cornell University, Ithaca, New York 14853-2501
(Received 6 February 1995)

The two strands of a closed circular DNA molecule possess as a topological invariant their linking number. This property, combined with an appreciable twist elastic constant, causes the double helix to assume a supercoiled conformation in space when a nonequilibrium twist is imposed. Thermal fluctuations play a crucial role in determining the conformation of supercoils, setting the linking number scale at which a well-defined interwound supercoil forms. In addition to equilibrium supercoil structure, we discuss supercoil bending and branching and show how at large scales supercoiled DNA becomes a branched polymer. The characteristic time required for intrasupercoil reactions to occur and the force necessary to extend twisted DNA are also derived.

PACS number(s): 87.15.−v

I. INTRODUCTION TO SUPERCOILING

Take a fairly stiff wire or string that is long enough to be loose and floppy — a shoelace is a good choice. Pull the two ends apart and twist the string five or six times. Naturally enough, you will feel a buildup of tension in the string. Now slowly bring the ends together without letting the string untwist. You should see that the string buckles and winds around itself as shown in Fig. 1(b): this interwound structure generally enters our lives as an annoyance, snarling our telephone cords and garden hoses.

Remarkably, circular double-helix DNA molecules from prokaryotes (cells without nuclear membranes, e.g., bacteria) and yeast often adopt the same sort of interwound structures, which are called "plectonemic supercoils" (from the Greek *plect*, meaning "braid," and *neme*, meaning "string"). The "super" reminds us that the size of these superhelices (typically 50 nm) is much larger than the double-helix repeat of the DNA molecule itself (3.4 nm).

The existence of supercoiled DNA was established by electron microscopy and sedimentation studies in the mid-1960s [1]. Later work showed that *in vivo*, even centimeter-long chromosomal DNA molecules contain "topological domains" along which supercoiling can occur, due to the attachment of the DNA to itself, cell membranes, and other large structures [2–4]. The existence *in vivo* of elaborate machinery for the manipulation of the topological state of DNA loops, through enzyme action and binding to particular proteins, further strengthens the conclusion that supercoiling of DNA plays a role in many biological processes [5,6].

The interwinding of a macroscopic string releases twisting strain: you can see the twist change as the string interwinds. This tradeoff is caused by a conserved topological charge, called the linking number, that can be partitioned into twisting or interwinding so as to minimize elastic energy. The linking number can be visualized for a string or tube by painting two stripes on opposite sides of the surface of the relaxed string. This is literally the situation for circular DNA molecules, where the role of the stripes is played by the two covalently bonded sugar-phosphate backbones [7]. If the string is closed into a loop so that each stripe forms a closed curve, they will be linked some integer number of times. The linking number (Lk) is a topological property: its integer value is conserved under smooth deformations. For a circular DNA molecule, Lk can be considered to be an experimental control parameter that determines the degree of supercoiling [8].

Here we expand a previously published description [9] of how thermal fluctuations compete with elastic forces to determine supercoil structure. Fluctuation effects dominate experimental results, setting the scale for Lk at which interwinding occurs, determining the super-

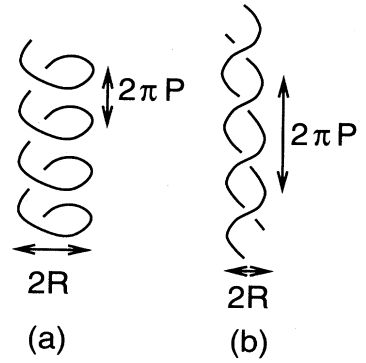

FIG. 1. Regular superhelices of pitch P and radius R; the solid lines represent double-helical B-DNA. (a) Solenoidal superhelix; (b) plectonemic superhelix.

coil structure, and causing branching of the plectonemic structure to occur [8]. Fluctuations also determine the kinetic pathways for intramolecular communication processes [10] that often occur between distant sites on supercoiled DNA molecules [11]. Supercoiled DNA cannot be understood without considering thermal fluctuation effects.

A. Unique physical properties of DNA and its organization

Double-helical DNA is a unique polymer. Unlike singly bonded main-chain polymers [e.g., polystyrene, poly(methyl methacrylate), and poly(dimethyl siloxane)] along which the backbone may be appreciably reoriented at a single bond [12], DNA is very stiff due to the tight constraint of successive pairs of nucleic acids ["base pairs" (bp)] by chemical and hydrogen bonds [13]. DNA has a thermal bending persistence length of about 150 bp (50 nm) [14]. The double-helical structure also has twisting rigidity, with a thermal twist persistence length of about 220 bp (75 nm) [15] (these elastic properties are for "standard" aqueous solution with $0.14M$ univalent salt). Twist rigidity is absent in most common singly bonded main-chain polymers where full rotation at any main-chain bond is possible and is crucial to the supercoiling effects described in this paper.

Well-defined interwound supercoils must be smaller than these thermal persistence lengths. Some sort of transition therefore will occur, from interwound supercoiling to more random conformations, when supercoil size approaches the persistence lengths. Thanks to the fact that these persistence lengths are long compared to the $\approx$ 2 nm effective radius of the DNA itself, there is a range of supercoil sizes that may be described using rather simple physics of elasticity and excluded volume without worrying about details of DNA-DNA interactions.

A variety of proteins carry out remarkably specific microscopic alterations of the double helix. For example, there are enzymes that act to ligate linear DNA molecules into circular form and enzyme complexes that replicate DNA. Another class of DNA-altering enzymes are the topoisomerases, which change circular DNA molecules from one topological isomer to another [5,6,16]. Topoisomerases may be roughly sorted into two categories based on how many sugar-phosphate backbones they break. Topoisomerase I breaks one backbone, introducing a transient "nick" that allows Lk to change while preserving the circular form of the molecule. Topoisomerase II grabs two pieces of double helix, completely cuts one of them, and passes the uncut double helix through the resulting gap, which is then sealed. By isolation and use of these enzymes *in vitro*, the topology of DNA can be manipulated [17] in ways that have no analog for other polymers.

At length scales of thousands of base pairs — half a micrometer of DNA — it becomes apparent that DNA *in vivo* is organized into topologically independent *loops*. In prokaryotes (bacterial cells and other single-celled organisms without a nucleus and other internal organelles) and in some yeast cells many circular *plasmid* DNA molecules of size 2 kilobp (kbp) to 10 kbp are found with linking numbers typically about 5% less than that of the relaxed double helix [18]. As we will see below, this Lk deficit is sufficient to cause supercoiling. The main part of the genome of many prokaryotic cells is organized as one large circular DNA of $\approx$ 2 megabp (Mbp). The circular genome of *Escherichia coli* has been shown to be organized into many loops of tens of kbp in length that are constrained at their ends by strongly bound proteins [2,19] and have linking number deficits of about 2.5%.

In eukaryotic cells (cells with nuclei and other organelles with their own internal membranes, the type making up yeast, fruit flies, humans, etc.) the long linear chromosomal DNA molecules are known to also be organized into loops [3–6]. These loops are proposed to extend between attachment points to the nuclear membrane and to the nuclear "protein scaffold" during interphase (the interval between cell divisions). During cell division the DNA molecules and various proteins condense to form well-separated pairs of (duplicate) daughter chromosomes that appear as X-shaped bodies in the light microscope. Inside each condensed chromosome, the DNA is believed to be organized into loops attached every $\approx$ 50 kbp to a central protein core.

The precise structure of eukaryotic chromosomes throughout the cell cycle is still mysterious, but it is well known that the linking number of DNA in eukaryotes is maintained at a linking number deficit of $\approx$ 5%. This is believed to be governed by the deformation of DNA when it is adsorbed to small protein complexes called histones [5]. DNA loops in eukaryotes should therefore supercoil when they are released from histones, but this has not been experimentally demonstrated. Supercoiling is thus likely relevant not only to *in vitro* experiments, which directly study the conformational properties of DNA loops of fixed length and Lk, but also to situations *in vivo*, where topological constraints on DNA loops may lead to supercoiling.

B. Previous work and this paper

Supercoiled DNA has been intensely studied from both experimental and theoretical perspectives [20]. The most complete quantitative experimental study of supercoil conformational structure as a function of Lk has been *in vitro* experiments of Boles *et al.* [8]. These experiments give compelling evidence that thermal fluctuations determine the structure of supercoils. Recent experiments of Bednar *et al.* [21] have indicated that counterions may play a role in mediating DNA-DNA attractions that may compete with fluctuation entropy.

When it was discovered that double-helix loops could be isolated in supercoiled form it was soon proposed that this could be understood in terms of a partition of Lk into twisting and interwinding components: Fuller [7] first outlined the basic physics of this problem. His insights led to a large body of work focused on the elastic part of the problem where thermal fluctuations are ig-

nored [22–24] and we now enjoy a deep understanding of the rich buckling behavior of twisted rods. This work has limited quantitative relevance to supercoiled DNA molecules that are longer than 1 kbp and take on random coil conformations when relaxed. The fluctuating supercoiled conformations that result as Lk is changed cannot be understood using elastic effects alone.

The pioneering theoretical study of fluctuation effects on supercoils is that of Vologodskii *et al.* [25–28], who have carried out large-scale numerical Monte Carlo (MC) simulations of the model that will be studied in this paper, the results of which are in quantitative accord with experiments. We have been strongly influenced by the MC results and our work is intended to be a complementary, analytical theory.

Section II of this paper describes the basic structural and elastic properties of DNA. A description of supercoils, supercoiling without thermal fluctuations, and ensembles for considering fluctuations follows. Section III describes chiral random coil conformations that occur for small Lk deficits. Supercoiling resulting from strong Lk changes are described in Sec. IV, where we introduce the idea of an entropic effective potential resulting from confinement of the polymer to a supercoil. We obtain a free energy from which supercoil properties are derived in agreement with results of experiments and MC simulations. In Sec. V we discuss the large-scale supercoil structure resulting from branching and bending fluctuations.

We have tried to advertise some of the possibilities for this field by devoting Secs. VI–VIII to models for specific experiments. Effects of supercoiling on intramolecular reaction kinetics are discussed in Sec. VI. In Sec. VII we show how extension of a twisted DNA molecule acts to bring solenoidal supercoiling into "phase coexistence" with plectonemic supercoiling; such effects should be experimentally observable via micromanipulation of single DNA molecules. Section VIII addresses the experiments of Bednar *et al.* [21] and shows how attractive interactions of modest strength can cause supercoil collapse.

II. DESCRIBING THE PROBLEM

Description of supercoiling requires knowledge of the basic physical properties of DNA. In this section we describe first the structure of DNA, a simple elastic model for weak distortions of the double helix, and a description of the electrostatic interaction between nearby DNA segments. We then discuss the linking topology of the double helix relevant to DNA loops. The idealized model of supercoils as regular helices will be introduced and used to show how the constraint of fixed linking number causes a twisted wire to buckle to form a supercoil. Finally, we will begin to address thermal fluctuations by introducing the ensembles that will be used to do calculations for loops with fixed linking number.

A. Structure and physical properties of *B*-DNA

We are exclusively concerned with the standard (*B*-form) double-helix DNA found *in vivo* [13]. Although there is some variation in the helix repeat distance with base-pair sequence, the unstressed *B*-DNA helix makes one turn about every 10.5 base pairs or roughly every $h = 3.4$ nm. The spatial angular frequency of the unstressed helix is $\omega_0 = 2\pi/h = 1.85\ \mathrm{nm}^{-1}$. The diameter of the double helix is about 2 nm.

The persistence lengths for bending and twisting are the natural length scales for thermal fluctuations and as mentioned above are 15–20 times h. The comparatively large energetic cost of disrupting the hydrogen bonded structure of the base pairs and their helical stacking means that the backbone or central axis of the molecule can be considered as inextensible and distances can be reckoned in either nm or bp. We imagine that on the lengths of interest, small irregularities of structure due to specific base pairs are averaged out and we do not consider the effects of strong intrinsic bends [29] [e.g., due to phased adenine-thymine (AT) pairs [30]].

1. Degrees of freedom

The degrees of freedom describing distortions of a DNA molecule may be separated into those defining the conformation of the central axis and those defining internal twisting of the double helix. We describe the axis with a space curve parametrized by arc length s, $\mathbf{r}(s)$. The tangent $\hat{\mathbf{t}} \equiv \partial_s \mathbf{r}$ is a unit vector that can be represented either by two angles or by the local Frenet-Serret curvature and torsion.

Twisting is measured by the spatial rotation rate of base pairs about the central axis, which for an undistorted DNA is just ω_0. Deviations in the twisting rate from ω_0 may be described using a scalar field $\Omega(s)$. This gives a total of three degrees of freedom per position s, exactly what is needed to describe an infinitesimal rotation of coordinate axes attached to each base pair as one moves down the molecule [31].

2. Elastic energy

Long-wavelength distortions of a *B*-DNA of length L may be considered to have an internal energy of the form

$$\frac{E_{\mathrm{el}}}{k_B T} = \frac{1}{2}\int_0^L ds\,\left[A(\partial_s^2 \mathbf{r})^2 + C\Omega^2\right]. \tag{1}$$

The first term is bending (curvature) elastic energy and is locally zero when the curvature $|\partial_s^2 \mathbf{r}|$ vanishes. The bending elastic constant A has been measured in a variety of ways to be about 50 nm for *B*-DNA [14] and may be defined by the decay of tangent correlations [32]: $\langle \hat{\mathbf{t}}(s)\cdot\hat{\mathbf{t}}(s')\rangle \sim \exp(-|s-s'|/A)$ for $|s-s'| \gg A$. The length A is therefore the persistence length for bending fluctuations.

The second term is the twisting elastic energy, which is nonzero when the double-helix twist is altered from ω_0. The twisting elastic constant C is rather less precisely known, but is believed to be roughly 75 nm [15]. The distance C is the twist persistence length and corresponds

to the distance over which a twist of 1 rad may be made with an energy cost of about k_BT.

This model is identical to that for weak distortions of a straight rod and is invariant under sign reversal of Ω. For the chiral B-DNA structure, the elastic energy must have some dependence on the sign of Ω [7], but this is a higher-order effect [31] important only when the bending radius is on the order of or less than the helix repeat h. Supercoiling bending radii are usually large compared to h, so in this paper we consider only the quadratic (1).

3. *DNA electrostatic interaction*

Each base is attached to a phosphate that is negatively charged in water. Conditions *in vivo* are aqueous solution with moderately high salt concentration (nominally $0.14M$ NaCl plus various other ions) and *in vitro* similar ionic conditions are typically used [8]. DNA-DNA interactions at intermediate ranges (1–3 nm) are therefore due to screened Coulomb interactions with a Debye-Huckel screening length of $\lambda_D \approx 1$ nm.

Our earlier paper [9] followed the lead of others [26] in replacing the electrostatic interactions with a short-ranged repulsion of range 1.75 nm. Because the entropy cost of confinement is much larger than the Coulomb interactions in typical supercoils, the precise form of the hard-core repulsion does not affect our results. Here we explicitly demonstrate this by using an accepted model for DNA electrostatic interaction instead of a hard-core interaction: the results of [9] are unaltered by this change.

The interactions of DNA molecules at ranges of 1–3 nm have been shown to be described by the Debye-Huckel interaction of charged rods [33–35] with an appropriately chosen effective electron charge per length ν [36]. For two parallel rods $2R$ apart, the interaction energy per unit length in units of k_BT is

$$w(R) = \ell_B \nu^2 K_0(2R/\lambda_D), \tag{2}$$

where the Bjerrum length (the distance at which unscreened Coulomb interactions equal k_BT) is $\ell_B = e^2/(\epsilon k_BT) = 0.7$ nm for water at 300 K. Here $K_0(x)$ is a modified Bessel function that decays exponentially for large x and diverges logarithmically for small x.

Poisson-Boltzmann theory and experiment [33,34] agree on appropriate values of the effective charge, which for $0.2M$, $0.3M$, $0.4M$, and $0.8M$ NaCl is $\nu = 9.0$, 10.9, 12.2, and 33.0 nm^{-1}, respectively. We will consider $0.14M$ NaCl solution with $\lambda_D = 0.8$ nm and $\nu = 8.4$. This model provides a convenient quantitative estimate of screened Coulomb interactions at medium-to-long ranges and a strong enough short-range interaction to disallow overlap of the B-DNA hard cores.

B. Topology of closed loops of DNA

The two strands of a circular DNA molecule possess as a topological invariant the number of times they wind around each other. This quantity is called the linking number. The linking number is integer valued, as can be seen by nicking one of the strands and allowing it to swivel around the other so that finally the DNA can be flattened into the plane with the base pairs radial and the two strands concentric circles. The number of rotations at the nick required to do this is an integer (half-integral values are disallowed as the strands have oppositely directed chemical structures [13]).

An unstressed B-DNA molecule has one right-handed twist per $h = 3.4$ nm along its length. When closed into a planar circle without twisting of the ends, the resulting linking number will be $\mathrm{Lk}_0 = L/h = \omega_0 L/(2\pi)$. Changes in Lk are conventionally measured relative to Lk_0 using either the excess linking $\Delta\mathrm{Lk} \equiv \mathrm{Lk} - \mathrm{Lk}_0$ or the fractional excess linking $\sigma \equiv \Delta\mathrm{Lk}/\mathrm{Lk}_0$. The intensive σ can be varied through roughly the range -0.1 to 0.1; beyond these bounds the double helix is unstable [20].

Lk is conveniently written as the sum of two geometrical quantities, neither of which is a topological invariant, but both of which are easily expressed analytically

$$\mathrm{Lk} = \mathrm{Tw} + \mathrm{Wr}. \tag{3}$$

The twist Tw is the integrated rotation of the internal degree of freedom about the molecule axis

$$\mathrm{Tw} \equiv \int_0^L \frac{ds}{2\pi}[\omega_0 + \Omega(s)] \equiv \mathrm{Lk}_0 + \Delta\mathrm{Tw}. \tag{4}$$

The constant term proportional to ω_0 counts up the linking number Lk_0 of the unperturbed double helix, while the twist strain (Ω) integral measures the excess or deficit rotation of the base pairs about the axis.

The writhe of the loop model described above is a simple function of only the molecule axis [7,20,37,38]

$$\mathrm{Wr} = \frac{1}{4\pi}\int ds \int ds' \frac{\partial_s \mathbf{r}(s) \times \partial_{s'}\mathbf{r}(s') \cdot [\mathbf{r}(s) - \mathbf{r}(s')]}{|\mathbf{r}(s) - \mathbf{r}(s')|^3}. \tag{5}$$

Wr is scale invariant and dimensionless and changes sign under reflection or inversion of $\mathbf{r}$, reflecting the cross product in the formula above. Therefore Wr= 0 if $\mathbf{r}(s)$ is planar or otherwise reflection symmetric.

A useful geometrical interpretation of Wr was derived by Fuller [39]. Given a configuration $\mathbf{r}(s)$, the tangent vector $\hat{\mathbf{t}}$ traces out a closed path on the unit sphere. Up to an integer offset that may be set by continuity, the writhe is equal to the total area $\mathcal{A}$ on the unit sphere enclosed by this path, divided by 2π,

$$\mathrm{Wr}|_{\mathrm{mod1}} = \left.\frac{\mathcal{A}}{2\pi}\right|_{\mathrm{mod1}}. \tag{6}$$

Right-handed and left-handed circulation on the sphere contributes positively and negatively, respectively, to $\mathcal{A}$.

The nature of the decomposition (3) can be grasped by manipulation of a long closed ribbon. First wind the ribbon into a planar spiral. The twist is zero as in the spiral region the base pairs running across the ribbon

from edge to edge are normal to the spiral plane. Now pull the ribbon ends out, without letting the ends rotate, so that the centerline of the ribbon becomes straight. The ribbon is now twisted, having the same number of twists as the original spiral had turns. The writhe of a straight line (or more properly a rectangle if the return loop is considered) is zero. The initial spiral plus connecting loop had writhe equal to the number of its turns that was converted into twist when pulled out.

C. Supercoils

The aforementioned experiments on wires, ribbons, and real supercoiled DNA motivate a model based on a regular right helix of radius R and pitch P (the helix repeat length is $2\pi P$; see Fig. 1) [40]. The length of molecule in 1 rad of superhelix is $\ell = \sqrt{R^2 + P^2}$. The helix angle γ is defined by $\sin\gamma = P/\ell$; we take γ to be between 0 (a circle) and $\pi/2$ (a straight line). Such a helix has constant curvature $\kappa = R/\ell^2$ and torsion $\tau = P/\ell^2$ [41].

A single-helix "solenoidal" supercoil [Fig. 1(a)] must be closed by, e.g., slow distortion of the coil into a toroidal structure. An interwound plectonemic superhelix [Fig. 1(b)] consists of two right helices of the same handedness that are interwound. At the ends of the resulting cylindrical structure, the two helices are connected. In the limit of $L \to \infty$, the effects resulting from the closure of the helix ends to form loops lead to a free energy correction that does not scale with L, which may be ignored in favor of the extensive bulk free energy.

The writhes of plectonemic and solenoidal coils are [38]

$$\mathrm{Wr} = \begin{cases} \mp 2n\sin\gamma & \text{(plectoneme)} \\ \pm n(1-\sin\gamma) & \text{(solenoid)}, \end{cases} \tag{7}$$

where n is the number of superhelix repeats, given by $n = L/4\pi\ell$ for the plectoneme and $n = L/2\pi\ell$ for the solenoid; the upper and lower signs reflect the result for right- and left-handed supercoils, respectively. The result for the solenoid for $\sin\gamma = 0$ can be seen to match the result of the ribbon experiment described in Sec. II B.

Per unit length of molecule, (7) is

$$\mathrm{Wr}/L = \begin{cases} \mp\tau/2\pi & \text{(plectoneme)} \\ \pm\tau[\sqrt{1+\kappa^2/\tau^2} - 1]/2\pi & \text{(solenoid)}. \end{cases} \tag{8}$$

Note that Wr is positive for left-handed plectonemes and negative for right-handed plectonemes; handedness versus Wr sign is opposite for the solenoid.

D. Collapse of supercoils at zero temperature

Using (8), one can immediately observe that at zero temperature, a long elastic wire or tube will collapse into a plectonemic supercoil when subject to the constraint $\Delta\mathrm{Lk}/L \neq 0$ [42]. To see this, first put all the ΔLk into Wr so that the twist energy is zero. Then collapse the plectoneme into a line (make $\sin\gamma = 1$, $\kappa = 0$), which makes the bending energy zero also. For a tube of nonzero radius, the elastic energy cannot be quite reduced to zero, but a plectoneme remains the preferred (lowest-energy) structure for tube radii that are small compared to superhelix pitch. For a solenoid, Wr is maximized for $\gamma = 0$ but the curvature of such a configuration is nonzero ($2\pi\Delta\mathrm{Lk}/L$ if $\Delta\mathrm{Tw} = 0$), so that both the twist and bend energies cannot be reduced to zero simultaneously.

Plectoneme formation (and the sign of the link formula) can easily be observed using a telephone: the cord between the handset and the cradle will form $n/2$ right- (left-) handed plectonemic repeats if n left- (right-) handed turns of the handset are made before it is hung up, assuming that the handset was picked up with the cord in a relaxed (unsupercoiled) configuration.

E. Fluctuation ensemble and linking constraint

Zero-temperature elastic energy arguments ignore thermal fluctuations that swell up the supercoil radius to larger than the DNA hard-core radius. We will show how a repulsive entropic effective potential arises, opposing the elastically driven collapse.

Conformation probabilities in thermal equilibrium are given by the Boltzmann distribution $\exp[-E_{\mathrm{el}}/k_BT]$. We want thermal averages done at fixed Lk, which may be done in either canonical or grand canonical Lk ensembles. The canonical ensemble treats Lk as fixed and will be used in most of this paper. The linking constraint may be enforced by the use of Tw=Lk−Wr to eliminate the twist from the elastic energy; this is is easily done since the twist field $\Omega(s)$ is a free Gaussian apart from this constraint. Numerical simulations of supercoiling generally employ this approach [25,26,43].

The grand canonical ensemble allows Lk to fluctuate, controlling its average value with a Lagrange multiplier — a chemical potential for linking number. The two ensembles are equivalent for large L since Lk fluctuations are only of order $(L/C)^{1/2}$. The grand canonical ensemble will be used solely to study "chiral random coils" in the next section.

III. CHIRAL RANDOM COILS

At finite temperature and small enough σ the $\sigma = 0$ random-coil loop conformation ensemble is only slightly changed and perturbation theory is reasonable. Since σ breaks chiral symmetry and introduces twisting strain into the loop we expect a slight chiral bias of the loop conformation in this regime.

We can roughly estimate the σ scale at which the chiral random coils become strongly distorted (i.e., where perturbation theory must fail) by noting that the $\sigma = 0$ chain is divided up into correlation regions of length C over which occur fluctuating contributions to Tw and Wr of order unity. The *added* linking per unit length is roughly $\omega_0\sigma$ and thus begins to compete with thermal effects when $|C\omega_0\sigma| \approx 1$. Since $C\omega_0 \approx 130$ we can expect perturbation theory to be valid for roughly $|\sigma| < 0.01$. In this regime, thermal fluctuations overwhelm the elas-

tic energy associated with the excess linking number. For larger $|\sigma|$ the elastic energy competes with the conformational entropy and can cause a gross reorganization of the coil — plectonemic supercoiling.

This constraint of fixed ΔLk may be imposed with a Lagrange multiplier μ in the grand canonical partition function

$$Z(\mu) = \int Dr \int D\Omega \exp\left(-\frac{E_{\rm el}}{k_B T} + \mu[\Delta{\rm Tw} + {\rm Wr}]\right). \tag{9}$$

For $\mu = 0$ Lk fluctuates freely. Twist and bend fluctuations are independent, so

$$\langle \Delta{\rm Tw}^n {\rm Wr}^m \rangle_0 = \langle \Delta{\rm Tw}^n \rangle_0 \langle {\rm Wr}^m \rangle_0. \tag{10}$$

The 0 subscripts refer to averages with $\mu = 0$. Both n and m must be even for this expectation value to be nonzero, since the energy is invariant under either of $\mathbf{r}(s) \to -\mathbf{r}(s)$ or $\Omega(s) \to -\Omega(s)$, which respectively change the sign of Wr and ΔTw.

Expansion of $\ln Z$ in μ gives

$$\ln Z = \ln Z_0 + \frac{\mu^2}{2}\left[\langle \Delta{\rm Tw}^2 \rangle_0 + \langle {\rm Wr}^2 \rangle_0\right] + O(\mu^4). \tag{11}$$

The mean-squared twist for $\mu = 0$ is

$$\langle \Delta{\rm Tw}^2 \rangle_0 = \frac{L}{(2\pi)^2 C}. \tag{12}$$

The mean-squared writhe is

$$\langle {\rm Wr}^2 \rangle_0 = \frac{\alpha L}{(2\pi)^2 A} \tag{13}$$

for some order-unity constant α [this follows from the exponential decay of correlations in $\mathbf{r}(s)$ with a correlation length of the bending persistence length].

The average twist and writhe for nonzero μ may be computed to linear order in μ from $Z(\mu)$,

$$\begin{aligned} \langle \Delta{\rm Tw} \rangle &= \frac{\mu L}{(2\pi)^2 C} + O\left(\frac{\mu^3 L}{C}\right), \\ \langle {\rm Wr} \rangle &= \frac{\alpha \mu L}{(2\pi)^2 A} + O\left(\frac{\mu^3 L}{A}\right). \end{aligned} \tag{14}$$

Thus $\Delta{\rm Lk} = \mu L(1/C + \alpha/A)/(2\pi)^2$ for small μ.

The partition of link into twist and writhe follows:

$$\begin{aligned} \langle \Delta{\rm Tw} \rangle / \langle \Delta{\rm Lk} \rangle &= \left(1 + \tfrac{\alpha C}{A}\right)^{-1} + O(\mu^2), \\ \langle \Delta{\rm Wr} \rangle / \langle \Delta{\rm Lk} \rangle &= \left(1 + \tfrac{A}{\alpha C}\right)^{-1} + O(\mu^2). \end{aligned} \tag{15}$$

Numerical calculations of Vologodskii *et al.* [26,44] for a DNA hard-core radius of 1.75 nm find ${\rm Wr}/\Delta{\rm Lk} = 0.72$ at $\Delta{\rm Lk} = 0$, giving $\alpha = 1.71$.

The Helmholtz free energy F at fixed linking number may be obtained by Legendre transformation

$$\frac{F}{k_B T} = -\ln Z + \mu \Delta{\rm Lk}, \tag{16}$$

which along with the definition $\sigma = 2\pi\Delta{\rm Lk}/(\omega_0 L)$ leads to

$$\frac{F - F_0}{k_B T L} = \frac{C\omega_0^2 \sigma^2}{2} \frac{1}{1 + \frac{\alpha C}{A}} + O(\sigma^4), \tag{17}$$

where F_0 is the free energy of the $\sigma = 0$ coil.

Precisely this behavior of the excess free energy has been observed experimentally [27,45] and in computer simulations [25,26], for supercoils with $|\sigma| < 0.01$. The experimental result of $F - F_0 \approx 10.0 k_B T N \sigma^2$, where N is the number of base pairs, when compared to the theoretical result, allows an independent estimate of C. Taking $A = 50$ nm and $\alpha = 1.71$ in (17) implies $C \approx 60$ nm, in reasonable agreement with other estimates [46].

When $|\mu|$ becomes of order unity this perturbative approach breaks down. Converting this to σ we find that perturbation theory is valid only for $|C\omega_0\sigma| < 1$: $X \equiv |C\omega_0\sigma|$ is the control parameter that measures the scale of σ. For $X > 1$ it will be shown below that plectonemic supercoiling occurs.

IV. FREE ENERGY OF SUPERCOILS

In this section we present a nonperturbative calculation of the free energy and structure of supercoils with $X \equiv |C\omega_0\sigma| \gg 1$. Our approach is variational and assumes that on average the backbone is a regular superhelix. On top of this regular structure we consider thermal fluctuations.

Superhelix formation puts a limit on the amplitude of the fluctuations (those that would cause the helix to intersect itself are disallowed), which in turn imparts a free-energy cost. This repulsive entropic effective potential sets the superhelix radius to be much larger than the DNA hard-core radius. This approach will be shown to be self-consistent for large X: the entropic potential calculation effectively decouples from the average elastic energy, giving a simple supercoil "equation of state."

In this section we will first indicate how fixed Lk can be used to find an effective Hamiltonian for the backbone fluctuations. We then carry out a simple scaling analysis to estimate the entropic potential. The same result is obtained in Appendix A in a more detailed calculation based on the superhelix normal modes.

A. Enforcing the fixed-linking number constraint

In the canonical fixed-Lk ensemble twist fluctuations (Ω) may be integrated out to yield an energy depending only on $\mathbf{r}(s)$,

$$\frac{E}{k_B T} = \frac{A}{2}\int_0^L (\partial_s^2 \mathbf{r})^2 + \frac{CL}{2}(\sigma\omega_0 - 2\pi {\rm Wr}[\mathbf{r}]/L)^2. \tag{18}$$

An uninteresting additive constant has been dropped. The constraint $\Delta{\rm Lk} = \Delta{\rm Tw} + {\rm Wr}$ has been directly employed to replace the integral $\Delta{\rm Tw} = \int ds \Omega/2\pi$. In principle, path integration of $\mathbf{r}(s)$ would give a complete description of supercoiling as a function of σ. Unfortu-

nately, the nonlinear long-ranged interaction inside Wr makes this procedure analytically problematic.

We will expand $\mathbf{r}(s)$ around a superhelical backbone configuration with constant curvature κ and torsion τ. The writhe is $\mathrm{Wr} = \mathrm{Wr}_0(\kappa,\tau) + \Delta\mathcal{A}[\mathbf{r}]/2\pi$, where Wr_0 is the writhe of the fixed-curvature–torsion superhelical reference state (8) and $\Delta\mathcal{A}/2\pi$ is the remainder, which if small is uniquely expressible in terms of the fluctuation in the area subscribed by the tangent vector on the sphere via (6). The exact form of Wr_0 will depend on whether the average superhelix is a solenoid, plectoneme, or some other structure.

The effective energy separates into constant and fluctuating parts

$$E = E_0 + \Delta E, \tag{19}$$

$$\frac{E_0}{k_BT} \equiv \frac{A\kappa^2 L}{2} + \frac{CL}{2}(\sigma\omega_0 - 2\pi \mathrm{Wr}_0/L)^2,$$

$$\frac{\Delta E}{k_BT} \equiv \frac{A}{2}\int_0^L ds[(\partial_s^2\mathbf{r})^2 - \kappa^2] - C(\sigma\omega_0 - 2\pi\mathrm{Wr}_0/L)\Delta\mathcal{A} + \frac{C}{2L}(\Delta\mathcal{A})^2.$$

Our aim is to estimate the free energy ΔF due to ΔE in order to compute the total free energy $F = E_0 + \Delta F$. Using simple scaling arguments we next show that the free-energy cost of confinement of the polymer in a supercoil can be obtained using an effective entropic potential (Appendix A derives the same results with a detailed calculation). To leading order in X only the curvature-squared fluctuations of (19) need be considered (Appendix B shows that writhe fluctuations give lower-order corrections).

B. Scaling derivation of entropic potential

Bending fluctuations that displace the DNA from its average position in a superhelix must be constrained to not disrupt it; this constraint leads to a free-energy cost dependent on the superhelix geometry. We find this free-energy cost using methods invented to compute the long-range repulsion of membranes arising from entropy loss [47]. These ideas have been applied to stiff polymers before: Helfrich and Harbich [48] and Odijk [49] considered the free energy due to confinement of a stiff polymer in a narrow tube; Podgornick and Parsegian examined the related entropic repulsive forces between DNA molecules in a nematic phase [34].

The rms displacement of a given point on a polymer or membrane diverges in the absence of a small-wave-number cutoff. Confinement of polymers or membranes sterically disallows such large fluctuations [47–49]; the size of the confining region determines the cutoff. The cutoff in turn determines the fluctuation correlation length and the entropy loss due to confinement.

For membranes and stiff polymers the energy of a mode of wave number q is Aq^4 times the square of the mode amplitude, where A is the bending elastic constant. For DNA inside a supercoil this power law is valid for large q and may by obtained by dimensional analysis of the fluctuation part of the bending energy $(\partial_s^2\mathbf{r})^2$. Equipartition for wave numbers larger than the cutoff ξ^{-1} gives a relation between the fluctuation amplitude r at any point on the membrane or polymer and the correlation length ξ,

$$r^2 \sim \int_{\xi^{-1}}^{\infty} \frac{d^D q}{Aq^4} \sim \xi^{4-D}/A, \tag{20}$$

where D is the dimension of the object (1 for polymers, 2 for membranes).

The fluctuation free energy is k_BT per correlation region. For membranes stacked with an average spacing r, the fluctuation energy per unit three-dimensional volume is the familiar Helfrich membrane interaction energy $k_BT/(Ar^3)$ [47]. For stiff polymers we have a free energy per length of $k_BT/(A^{1/3}r^{2/3})$: this is the entropy cost of either confining a stiff polymer between plates of separation r or inside a tube of radius r [48,49]. The entropy cost diverges in either case for $r \to 0$ as the cutoff moves to progressively higher wave numbers.

In the stiff polymer case this argument is limited to $r < 2A$. For $r \approx 2A$ the free energy is $\approx k_BT/A$, which, interpreting $2A$ as the step length of an equivalent *flexible* polymer, is precisely the free-energy loss that we would expect in maximal confinement of a flexible polymer: about k_BT per step. For $r > 2A$ the polymer is described by a conventional random-walk polymer model and its confinement free energy can be computed using the Edwards model for a flexible chain with a monomer size of $2A$.

In the case of a supercoiled stiff polymer (DNA), we apply this argument to the normal modes of a helical structure. Cutoffs on the resulting spectrum are set so that a given point on the coil has radial displacements of order R and displacements along the supercoil axis of order πP. The confinement free energy per unit length therefore has leading divergences for small R or P of the form

$$\frac{\Delta F}{k_BTL} = \frac{1}{A^{1/3}(\pi P)^{2/3}} + \frac{1}{A^{1/3}R^{2/3}}. \tag{21}$$

The same result is obtained in Appendix A in a more detailed calculation using the normal modes of a superhelix.

C. Supercoil free energy

The total supercoil free energy is obtained by adding elastic [E_0 from (19)], entropic (21), and electrostatic (2) contributions

$$\frac{F}{k_BTL} = \frac{A}{2}\kappa^2 + \frac{C}{2}\left(\sigma\omega_0 - \frac{2\pi\mathrm{Wr}_0}{L}\right)^2 + \frac{1}{A^{1/3}(\pi P)^{2/3}} + \frac{1}{A^{1/3}R^{2/3}} + w(R) + w(\pi P). \tag{22}$$

The free energy depends on two parameters R and P (equivalently κ and τ), whose equilibrium values must be determined by minimization of (22). A comparison of

the free energies of competing structures (e.g., the plectoneme and the solenoid) will determine the stability of these candidate "phases."

The free energy (22) used in this paper is symmetric under $\sigma \to -\sigma$ and $\tau \to -\tau$: states with opposite signs of σ are related by inversion. This symmetry is not exact as the B-DNA double helix is chiral. However, for scales larger than the helix repeat, relevant to supercoiling, chiral-symmetry-breaking elastic energy terms first occur at nonlinear order and will lead to rather weak effects [31]. Therefore it suffices to present our results as a function of $|\sigma|$ leaving the sign of σ to determine the handedness of the energy-minimizing state; $\sigma < 0$ favors right-handed plectonemes or left-handed solenoids and for $\sigma > 0$ the reverse.

D. Supercoil equation of state

Plectonemic supercoil ($\sigma < 0$) properties may be computed by inserting $2\pi \mathrm{Wr}_0/L = -\tau$ into (22) and numerically minimzing the free energy to determine R and P. For $|\sigma| < 0.020$, the minimal free-energy state has $R = P = \infty$, indicating that no consistent (stable) supercoiled state exists for small $|\sigma|$. For $|\sigma| > 0.020$, a minimum appears in the plectoneme free energy for finite R and P, indicating the appearance of a stable supercoiled state. The free energy of this state grows approximately linearly with $|\sigma|$, slower than that of the $R = P = \infty$ unwrithed state, which is $C(\sigma\omega_0)^2/2$ (see Fig. 2).

The plectoneme free energy crosses that of the unsupercoiled state at $|\sigma| \approx 0.023$ ($X \equiv |C\omega_0\sigma| = 3.0$), leading to a "first-order" phase transition in our model. The plectoneme radius R is shown on the top of Fig. 3; at the point where the plectoneme free energy crosses the unsupercoiled state ($|\sigma| = 0.023$) $R = 26$ nm; for larger $|\sigma|$, R decreases, approaching ≈ 2 nm for $|\sigma| > 0.08$. The lower part of Fig. 3 shows the number of turns per unit length, which in our model is just $1/[2\pi(R^2 + P^2)^{1/2}]$. This quantity increases roughly linearly with $|\sigma|$.

In Fig. 4 we show two more properties of the plectoneme state (solid curves); on the top we show $\mathrm{Wr}/\Delta\mathrm{Lk}$, which starts out around 0.4 at $|\sigma| = 0.023$ and then quickly rises to about 0.8 at $|\sigma| = 0.06$. It then slowly decreases for large $|\sigma|$. Our model does not include a crossover from a fluctuating plectoneme to a chiral random coil: if this were done $\mathrm{Wr}/\Delta\mathrm{Lk}$ would go smoothly to ≈ 0.7 for $|\sigma| < 0.01$. The length of the superhelix axis as a fraction of $L/2$, which in our model is just $\sin\gamma$, is shown in the lower half of Fig. 4; this quantity is between 0.84 and 0.94 over the whole $|\sigma|$ range; this corresponds to a superhelix opening angle γ between 57° and 70°.

Much of the behavior of (22) can be understood by noting that the length scale $\ell = (R^2 + P^2)^{1/2}$ characterizes R and P (it is the chain length containing 1 rad of superhelix). As a function of ℓ^{-1}, the free energy always has a minimum at $\ell^{-1} = 0$ because of the nonanalytic fluctuation term $1/(A^{1/3}\ell^{2/3})$, $\partial F/\partial(\ell^{-1}) > 0$. For larger ℓ^{-1}, the negative σ-dependent term in the elastic energy $A/\ell^2 - |C\sigma\omega_0|/\ell$ may cause the free energy to decrease before the quadratic curvature energy term takes over. Thus, for large enough $|\sigma|$ there is a second smooth local minimum in F, which may become the global minimum causing ℓ^{-1} to jump from zero to something finite. This analysis indicates that supercoil stability is not dependent on the short-ranged electrostatic interaction terms

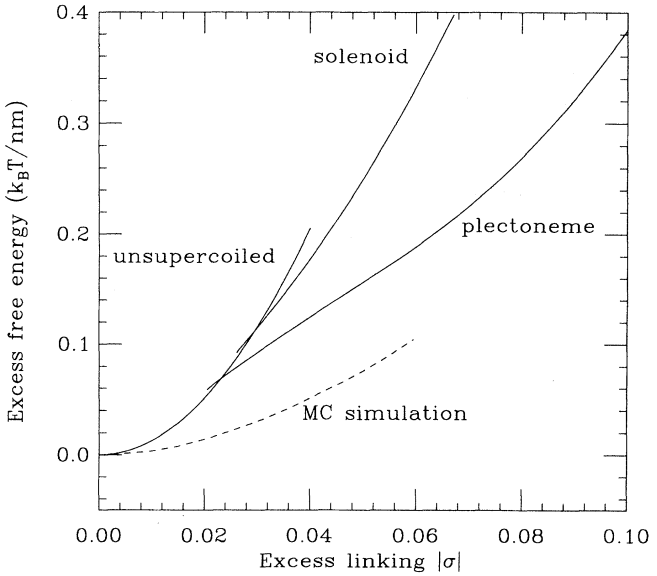

FIG. 2. Free energies of plectonemic and solenoidal supercoils compared with unsupercoiled state. The solid line marks the result of (22); the dashed line indicates the Monte Carlo result of Vologodskii *et al.* [26].

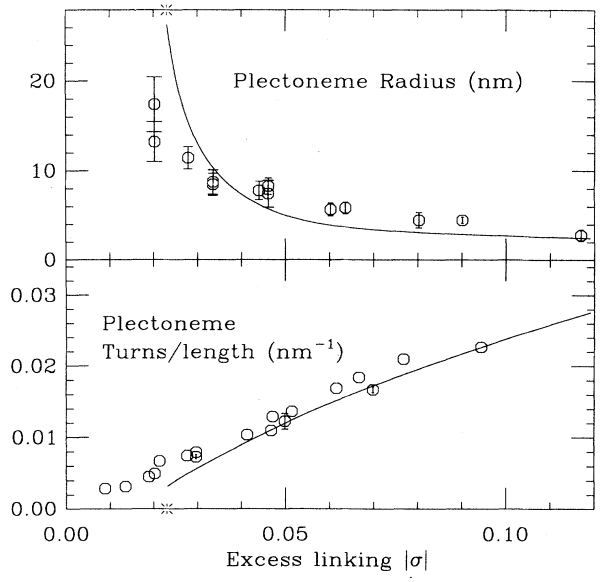

FIG. 3. Radius R (top) and superhelical turns per length $(2\pi[P^2 + R^2])^{-1/2}$ (bottom) of plectonemic supercoils. Solid lines indicate the result of minimization of free energy (22); symbols indicate the experimental results of Boles *et al.* [8]. The star on the $|\sigma|$ axis marks where the plectoneme becomes the most stable state.

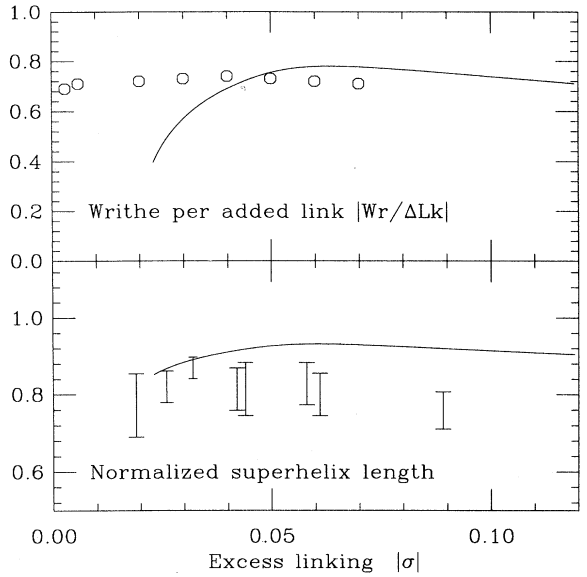

FIG. 4. Writhe per added linking (top) and superhelix axis length divided by half of the DNA length (bottom) for plectonemic supercoils. Circles are Monte Carlo results of Vologodskii *et al.* [26], while bars give experimental results of Boles *et al.* [8]. Solid curves are our theoretical results.

except implicitly, through the entropic potential. The electrostatic interaction is important only for sufficiently large $|\sigma|$ so that either R or P is reduced to the point where $w(R)$ or $w(\pi P)$ dominates the free energy.

The first-order nature of the transition, along with the fact that the total linking number is fixed, suggests that there should be pseudophase coexistence of random coil and supercoil near the transition, even though fluctuations will eliminate any true phase transition [even though Wr generates a long-ranged interaction, its contribution to (22) only scales as L and cannot generate a true phase transition [50]]. A final point about the transition is that it involves no spontaneous symmetry breaking since chiral symmetry is already broken for chiral random coils (i.e., for any $\sigma \neq 0$).

To examine solenoidal supercoiling, we use the solenoid writhe $2\pi \mathrm{Wr}_0/L = \tau[(1+\kappa^2/\tau^2)^{1/2} - 1]$ and again proceed numerically. Again, for small $|\sigma|$, the nonanalytic entropic term causes the free energy to only have a minimum at $R = P = \infty$ and again a new local minimum appears at finite R and P at $|\sigma| = 0.026$. Although the solenoid free energy is lower than that of the $R = P = \infty$ unsupercoiled state for $|\sigma| > 0.029$, it grows $\sim C(\sigma\omega_0)^2$ and as a result is never below the plectoneme free energy (Fig. 2). The solenoid writhe is small unless there is appreciable curvature [$\mathrm{Wr}_0(\kappa = 0) = 0$ for the solenoid]. Solenoidal supercoiling thus cannot fully compensate added linking number without introducing bending energy, leading to a quadratic $|\sigma|$ dependence.

1. *Scaling limit for plectoneme*

We now examine the free energy in the regime where the direct hard-core interactions are not contributing significantly to the free energy, which occurs for DNA plectonemes at 140 mM NaCl when $R \gg 2.5$ nm or for $|\sigma| < 0.08$. We consider the case where $\sigma < 0$ for definiteness. We drop hard-core terms, suppose $P \gg R$, and drop the $P^{-2/3}$ term, giving

$$\frac{F}{k_B T L} = \frac{A}{2}\kappa^2 + \frac{C}{2}\tau^2 + \frac{X^2}{2C} - X\tau + \frac{1}{A^{1/3}}\frac{\tau^{4/3}}{\kappa^{2/3}}, \quad (23)$$

where $X \equiv |C\omega_0\sigma|$. *A posteriori* it will be shown that the other fluctuation contributions can be ignored.

The free energy should be minimized with respect to τ and κ. The minimum is at

$$\begin{aligned} \kappa &= X_0^{1/2}(X - X_0)^{1/2}/(2AC)^{1/2}, \\ \tau &= (X - X_0)/C \end{aligned} \quad (24)$$

for $X \geq X_0 = 2(2/3)^{3/4} \approx 1.5$. At $X = X_0$ the supercoiled state ceases to be consistent and κ and τ become zero, as in the numerical treatment of the full free energy. In the scaling regime $X \gg 1$, $\tau \gg \kappa$, indicating that the superhelix has $R \ll P$, as we expect from the zero-temperature plectoneme collapse discussed earlier. The scaling supercoiling free energy at this minimum grows linearly with X:

$$\frac{F}{k_B T L} = X_0^2/(2C) + X_0(X - X_0)/C. \quad (25)$$

We note that for large X this is far less than the free energy of an unwrithed coil with linking number made up by twist $X^2/(2C)$.

We now summarize the scaling with X of various quantities at the plectonemic scaling minimum. Correction terms and numerical order-unity corrections to amplitudes are ignored. For $X \gg 1$ the pitch scales inversely with X:

$$P \sim 1/\tau \sim C/X. \quad (26)$$

Plectoneme radius also scales inversely with X, but with a stronger exponent

$$R \sim C^{3/2}/(A^{1/2}X^{3/2}). \quad (27)$$

The upper limit $X_{\max}$ for application of the scaling free energy can be estimated by noting when the radius (27) approaches the effective hard-core radius $R(X_{\max}) \approx 2$ nm (Fig. 3, top). This occurs for $X_{\max} \approx 11$, corresponding to $|\sigma_{\max}| \approx 0.08$.

We now justify the gradient expansion used in the derivation of the entropic potential. The correlation length for the fluctuations is related to their free energy per length $F/L \sim k_B T/\xi$, thus $\xi \sim C/X \sim P$. This should be compared to the amplitude of the radial fluctuations

$$\langle \delta r^2 \rangle \sim \xi^3/A \sim C^3/(AX^3). \quad (28)$$

For large X we see that $\langle \delta r^2 \rangle \ll \xi^2$ and that our expansion is reasonable. Further, $\langle \delta r^2 \rangle \approx R^2$, indicating that R is consistently determined by the radial fluctuations. The fluctuations in the z direction (along the plectoneme

axis) are on the same order and are much less than P^2 for large X, indicating that the fluctuations in the z direction are not important.

We can also estimate the writhe per unit length $\mathrm{Wr}/L \approx -X/(2\pi C)$. We note that $\Delta\mathrm{Lk}/L = \sigma\omega_0/(2\pi) = -X/(2\pi C)$ and therefore that $\mathrm{Wr}/\Delta\mathrm{Lk} \approx 1$ for X large. This reflects that it is energetically favorable for the linking number to be entirely made up by writhe in the case of the plectoneme. The hard-core interactions will reduce the maximum value that $\mathrm{Wr}/\Delta\mathrm{Lk}$ can take on for $X > X_{\max}$, as seen in the complete numerical calculation (see the top of Fig. 4).

The pitch-dependent part of the entropic repulsion may be ignored for large X, since it is of order $\kappa^{4/3}/(A^{1/3}\tau^{2/3}) \sim 1/A$. This approaches a constant value for large X and is negligible compared to the scaling part of the free energy in the scaling regime.

2. *Scaling limit for the solenoidal supercoil*

The scaling free energy for the solenoid for $X \gg 1$ has the form

$$\frac{F}{k_BTL} = \frac{A+C}{2}\kappa^2 + \frac{C}{2}\tau^2 + \frac{X^2}{2C} + \frac{1}{A^{1/3}}\frac{\kappa^{4/3}}{\pi^{2/3}\tau^{2/3}}. \quad (29)$$

Again, the hard-core terms have been dropped and $P \ll R$ has been assumed.

Minimization with respect to κ and τ for $X \gg 1$ leads to

$$\kappa \approx X/(A+C), \quad (30)$$
$$\tau \approx \frac{X_0^{1/2}}{2^{1/2}\pi^{1/4}A^{1/8}C^{3/8}(A+C)^{1/2}}X^{1/2}.$$

We see that $\kappa \gg \tau$ for $X \gg 1$, justifying the choice of terms kept above. The radius and pitch are readily computed

$$R \sim 1/\kappa \sim (A+C)/X, \quad (31)$$
$$P \sim \tau/\kappa^2 \sim A^{1/8}C^{3/8}/[(A+C)^{3/2}X^{3/2}],$$

i.e., for $X \gg 1$, $R \gg P$.

The scaling part of the solenoid supercoiling free energy behaves as

$$\frac{F}{k_BTL} \approx \frac{A}{A+C}\frac{X^2}{2C}, \quad (32)$$

which we see is much larger than that of the plectonemic supercoil for $X \gg 1$. The writhe of the solenoid for large X is

$$\mathrm{Wr}/L \approx -\kappa/(2\pi) \approx -X/(2\pi[A+C]) \quad (33)$$

or in terms of the added linking number $\mathrm{Wr} \approx [C/(A+C)]\Delta\mathrm{Lk}$. Thus solenoidal writhe can only partially compensate for added linking number and the leftover Lk must be made up by Tw, causing the free energy to rise quadratically with X. This large static energy dominates the total solenoidal free energy.

The fluctuations are characterized by a correlation length of

$$\xi \sim A^{1/3}\tau^{2/3}/\kappa^{4/3} \sim (A/C)^{1/4}(A+C)/X, \quad (34)$$

which is large compared to the fluctuations in the z direction of order P, consistent with the use of the Gaussian approximation for the curvature fluctuations. The radial fluctuations scale as $\delta r^2 \sim \xi^3/A \sim (C+A)^3/(AX^3)$, which is much less than the solenoid radius of $R^2 \sim (C+A)^2/X^2$ for large X.

E. Comparison with experiments and Monte Carlo simulations

Three groups have provided data with which we can compare our results. The first two [8,21] have carried out experiments on circular DNA molecules called plasmids, which carry small groups of genes in bacteria and yeast. Plasmids can be isolated from a cell, stripped of all proteins, and processed enzymatically so as to alter their linking number. The result is that circular DNA molecules with controlled σ can be produced *in vitro*. The two experimental groups have visualized supercoiled plasmid structure using electron microscopy (EM). The third group has carried out large-scale Monte Carlo simulations of such plasmids [25–28].

1. *Study of supercoiled DNA and its recombination products on an EM grid*

Boles *et al.* [8] used 7 kbp plasmids ($L \sim 2400$ nm) with $-0.089 \le \sigma \le 0$ and 3.5 kbp plasmids with $-0.117 \le \sigma \le -0.019$. The number of superhelical turns and the length of superhelix axis were determined by room temperature electron microscopy. The superhelix radius was inferred from these two measurements by assuming a regular plectoneme and correcting for end effects. The linking number was adjusted by nicking the plasmid (i.e., cutting one of the strands), adding an intercalating dye that lengthens the double-helix period, and letting excess twist relax. The DNA is then resealed, the dye is removed, and the linking deficit appears. The delicate point is then to show that the supercoiling or writhe in solution gets just linearly projected onto the EM grid when the "spreading solution" is removed.

A complementary and very elegant enzymatic technique was used on variants of the smaller plasmids, to convert the number of superhelix turns in solution into a topological property that is unaltered by whatever is then done to prepare the EM picture short of breaking the molecule. An enzyme called Int, responsible for site specific recombination, can cut, swap, and reseal two pieces of double-stranded DNA at special sites called *attP* and *attB* [Fig. 5(a)]. Depending on how the sequences are ordered, either a toroidal knot or two catenated rings are formed, with an order equal to the number of supercoils between the sites [Figs. 5(b) and 5(c)]. The topology of the resulting structure is easily discerned by EM.

Visualization of the supercoils indicated that, for $|\sigma|$ between 0.019 and 0.120, they had a well-defined interwound plectonemic structure. For $|\sigma| < 0.016$, it was observed that "most molecules have an irregular shape" (Ref. [8], p. 946). We interpret this observation as a verification of our idea that there is a transition from a chiral random coil to a plectonemic supercoil for $\sigma \approx 0.023$. The pictures shown in Fig. 6 of Ref. [8] for $\sigma = -0.016$ are suggestive of phase coexistence between plectoneme and random coil states, as one would expect near such a first-order transition.

The experimental data for the number of superhelical turns per length from the recombination assay are shown in the lower part of Fig. 3, along with our theoretical result for $1/[2\pi(R^2 + P^2)^{1/2}]$ vs σ. Most of the range of data is unaffected by specifics of the hard-core interaction in the theory (compare this figure with Fig. 2 of Ref. [9], which uses a different hard-core interaction) and follows the scaling law $1/P \sim C/X$ since $P \gg R$. As can be seen from Fig. 3, our model *with no fit parameters* agrees remarkably well with the experimental data for the number of turns per unit length.

Experimental measurements of the superhelix axis length for the 7 kbp plasmid, normalized by one-half of the total DNA length, are plotted versus $|\sigma|$ in the lower half of Fig. 4. This ratio, equal to $\sin\gamma = P/[P^2+R^2]^{1/2}$ in our theory, is shown with the solid line. One can see that this quantity varies only slightly with σ and that again theory and experiment are in reasonable agreement. Our theoretical estimate does not take into account the effect of the plectoneme ends and branches, which could account for the fact that the theoretical superhelix length slightly exceeds that observed experimentally.

The average plectoneme radius (inferred in Ref. [8] from axis length and turns per length) is shown in the upper half of Fig. 3 along with our theoretical result. For large σ the data approaches a value of about 2.5 nm, sim-

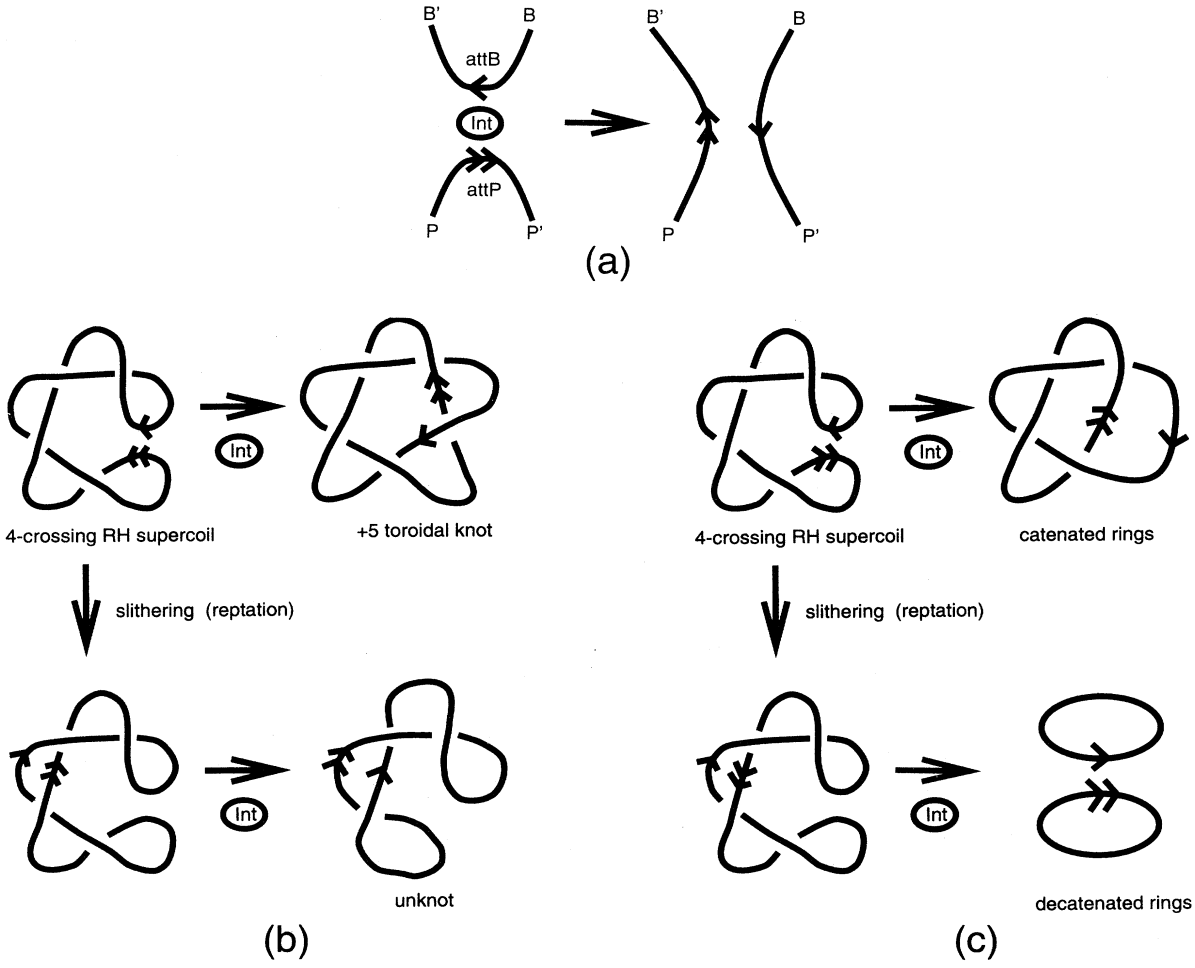

FIG. 5. Site-specific recombination reactions can convert geometrical properties of supercoiling into topological ones. (a) The enzyme Int locally switches aligned *attP* and *attB* sequences. If the *att* sequences are in (b) "inverted repeat" or (c) "direct repeat" on a supercoiled DNA molecule, Int generates a toroidal knot (for the supercoil shown, either a +5 or +3 knot could result, depending on how the DNAs were crossed) or two catenated rings, respectively, with knotting or catenation determined by the number of superhelical turns between the *att* sites at the moment of the reaction. This figure is adapted from Ref. [55].

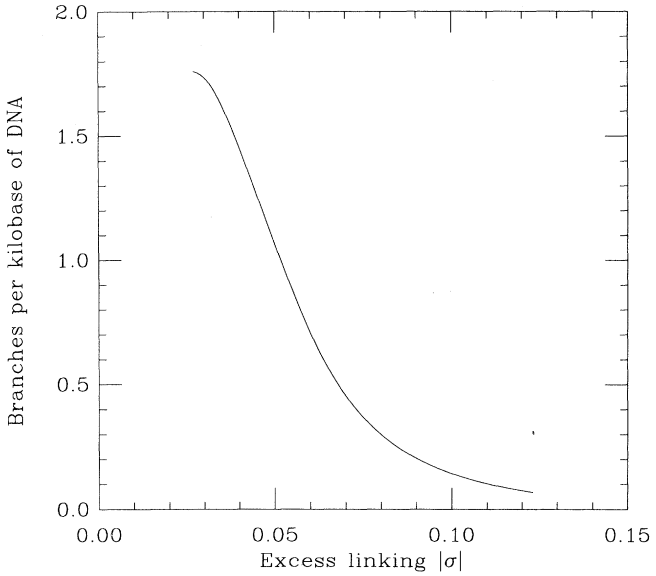

FIG. 6. Numerical estimate of the number of branches per kilobase of DNA from (35) that neglects the repartition of σ between the branch and plectoneme regions.

ilar to the effective hard-core radius expected for DNA in $0.14M$ NaCl. For smaller σ where the experiments fit a $R \sim 1/\sigma$ law, the theory gives no simple scaling because of proximity to the transition point at $|\sigma| = 0.023$. Although the experiments for R have sizeable error bars, it is unreasonable that Coulomb or other purely energetic effects could be responsible for the swelling of the plectoneme coils.

In addition to these quantities, Boles *et al.* [8] also measured the number of branching points along the plectonemic axis. We will defer discussion of these results to Sec. VI B.

2. *Cryo-EM visualization of supercoiled DNA*

A different visualization method was used in recent experiments of Dubochet *et al.* [21]. Again, the objective was to determine the in-solution structure of 2.7 kbp plasmids with native supercoiling $\sigma \approx -0.046$ ($X \approx 6.4$, well into the regime where plectonemic supercoiling should be stable). However, instead of adsorption of the DNA onto a surface, a drop of DNA solution was spread onto a perforated carbon film and cooled to $-172\,^{\circ}$C in about 100 μsec. The solution vitrifies (forms an amorphous glassy solid) and one hopes that everything in it, in particular the DNA, is immobilized in conformations representative of the 25 °C solution. The sample is then transferred to an EM stage for study, all at $-172\,^{\circ}$C.

The results of these studies, which focused not on variation of σ but rather on variation of salt concentration, are remarkable. In 10 mM TRIS-HCl (screening length ≈ 3 nm), a superhelix radius of 6 nm, a superhelix opening angle of $55^{\circ} \pm 6^{\circ}$, and $\mathrm{Wr}/\Delta\mathrm{Lk} = 0.78$ were observed, roughly consistent with the results of Boles *et al.* and consistent with our model for plectoneme swelling by thermal fluctuations. In 10 mM NaCl, a similar structure was observed.

However, for $\geq$ 100 mM NaCl (screening length $\approx$ 1 nm) or $\geq$ 10 mM $MgCl_2$, the two double strands of DNA in the plectoneme could not be resolved, suggesting that the structures had collapsed. Granting that the cryo-EM technique is without serious artifacts, DNA collapse at these ionic strengths is superficially at variance with other macroscopic studies of linear DNA molecules in solution at ionic strengths $\sim$ 10 times higher [34,35] (where multivalent cations are required for collapse [35,51]). A possible resolution of this conflict suggested in [21] is to suppose that the supercoiling at large linking numbers removes enough of the configurational entropy to allow a small attractive component in the otherwise entropy-dominated free energy to trigger collapse. A calculation along these lines is given in Sec. VIII. There remains a potential conflict with [8], which observed no collapse for nearly comparable ionicities.

3. *Monte Carlo simulation of supercoiled DNA*

MC simulations appropriate to room temperature of the standard model (1) with the twist fluctuations eliminated in favor of the imposed Lk and backbone Wr (Sec. II E) have been done by Vologodskii *et al.* [25–28]. They took A =50 nm, C =75 nm and a hard-core DNA radius of 1.75 nm and were able to treat plasmids in the range 2.7–10 kbp. The degree of quantitative agreement with the experiments of [8] is a validation of both the theoretical model and the experimental protocols. Well defined plectoneme superhelices occur for $|\sigma| \geq 0.02$, while only random coils are seen for smaller $|\sigma|$. This observation is quantified in Fig. 14 of [26], where the entropy of the backbone configuration is shown to remain at its $\sigma = 0$ value for $|\sigma| \leq 0.02$. Both observations are consistent with our transition at $\sigma = 0.023$.

The MC free energy per length of DNA vs σ [25,26] is graphed in Fig. 2 and sits a few k_BT/A below our values for the plectoneme. This is to be expected since we have neglected random walking of the plectoneme axis, which would contribute an entropy of this amount. The simulations also agree very well with the experimental data shown in Figs. 3 and 4 and therefore with our theory. The only problem occurs in $\mathrm{Wr}/\Delta\mathrm{Lk}$ near the transition where our theory does not describe the crossover to a random chiral coil properly.

V. LARGE-SCALE STRUCTURE OF SUPERCOILED DNA: BENDING AND BRANCHING FLUCTUATIONS

Experiments and simulations show that plectonemic supercoils undergo bending fluctuations and that there is a certain probability of having a branch at any turn of the superhelix, indicating that long plectonemes should behave as flexible branched polymers. We will argue that for short DNA molecules, a linear plectoneme with Gaussian statistics and radius of gyration $R_g \sim L^{1/2}$ is ex-

pected; for DNA larger than a few kbp, branching occurs and the polymer is a Zimm-Stockmayer [52] Gaussian branched polymer with $R_g \sim L^{1/4}$; for DNA molecules larger than about 25 kbp, self-avoidance is important and one returns to a regime where $R_g \sim L^{1/2}$ [53]. The overall supercoil size R_g (not to be confused with the much smaller plectonemic radius R) is of interest as it determines transport mobilities and chain rearrangement times.

A. Short supercoiled DNA molecules are Gaussian polymers

The plectonemic backbone in the absence of branching can be considered as a persistent chain polymer, with an effective bending rigidity of about $2A$ and therefore with an effective monomer length [32] of $b = 4A$. The number of statistically independent segments in an interwound plectoneme will be $N = L/(2b)$ and the excluded volume of a segment will be $\approx 2b^2R$, where $R \sim C/X^{3/2}$ is the plectoneme radius. Application of Appendix D to this effective linear polymer shows that excluded volume effects are only an issue for L so long that branching occurs; short supercoils will be random walks with $R_g \approx (2AL)^{1/2}$.

B. Longer supercoiled DNA molecules are branched polymers

Very general statistical mechanical arguments indicate that plectonemic supercoils must branch. Namely, the entropy gained in creating a branch grows as $\approx \ln(L)$ for large L, while the energy cost is finite. The branch spacing λ will be just that length for which the entropy gain balances the energy loss for an additional branch. Suppose that 2 rad of superhelix (total length $2\ell = 2[P^2 + R^2]^{1/2}$ Sec. II C) must be converted to random coil to create the junction and that this can occur in $(L/2\ell)$ independent places along the plectoneme. The energy cost can be estimated from the difference in free energies per length for the two states in question from Fig. 2. Thus λ is determined by

$$\ln\left(\frac{\lambda}{2\ell}\right) \approx \frac{2\ell\Delta F}{k_BTL} \tag{35}$$

and is shown in Fig. 6.

For moderate $|\sigma| \leq 0.06$, we find about one branch per kbp or $\sim$ 330 nm, compared with something closer to $\lambda \approx 500$ nm in simulations [27] and $\lambda \approx 800 \pm 200$ nm in experiments [8]. Since the error in our energy estimate occurs in the exponent when (35) is solved for λ, we consider this agreement reasonable. We adopt the value $\lambda = 1000$ nm in subsequent estimates: the formulas below depend rather weakly on λ. The rapid growth in λ predicted by (35) for $|\sigma| > 0.06$ is spurious since the average σ was assumed for the chiral coil region in estimating ΔF. In reality, σ will shift from coil to plectoneme in the same way as occurs in the region of chiral coil-plectoneme coexistence near the transition at $X \approx 3.0$. Thus λ should be largely independent of σ.

The branching pattern of plectonemic DNA is not frozen for $L > \lambda$, but rather is fluctuating and in thermal equilibrium, a very unusual circumstance for polymers of fixed chemical structure. Zimm and Stockmayer [52] have estimated the radius of gyration of such a structure (often called a "lattice animal") when self-avoidance is immaterial:

$$R_g \approx b(\lambda N/b)^{1/4} \approx A(8L\lambda/A^2)^{1/4}. \tag{36}$$

Doaud and Joanny [53] used Flory theory to determine where, i.e., at what L, self-avoidance becomes important and the scaling of R_g at larger L. They posit a free energy

$$\frac{F}{k_BT} \approx \frac{R_g^2(b/\lambda)^{1/2}}{b^2N^{1/2}} + \frac{b^2RN^2}{R_g^3}, \tag{37}$$

where the first entropic term restates the Zimm-Stockmayer result, while the second term is the free energy cost of self-avoidance for N segments of length b and radius R in a volume R_g^3 (Appendix D). Therefore self-avoidance enters the problem when the second term is ≈ 1 when estimated with R_g from (36) or for $L > 8A(2A/R)^{4/5}(\lambda/4A)^{3/5}$. Using $R = 8$ nm, $\lambda = 1000$ nm, and $b = 4A$ we find this crossover at $L \approx 8 \times 10^3$ nm or 2.4×10^4 bp. Note that there are only eight branches at this crossover and L is $5 - 10$ times shorter than the analogous crossover for unsupercoiled DNA (Appendix D). The greater density implied by (36) compared to a random walk is responsible for the difference.

In the presence of self-avoidance the radius of gyration is found by balancing the two terms in (37),

$$R_g \approx A\left(\frac{R}{2A}\right)^{1/5}\left(\frac{\lambda}{4A}\right)^{1/10}\left(\frac{2L}{A}\right)^{1/2}. \tag{38}$$

There are thus two points at which the statistics of the coils change and for our parameters, they occur at ≈ 3 kbp and ≈ 25 kbp, precisely bracketing the range where experiments are likely to be done. In this regime, $R_g \sim L^{1/4}$, while for either larger or smaller chains, we expect the random walk scaling $R_g \sim L^{1/2}$. Thus experiments or simulations to determine the size of supercoils should be done with several L per decade; fewer data points could be quite misleading.

MC simulations for various L have been done [25–28], but $R_g(L)$ plots are unavailable. The only plot of R_g is versus $|\sigma|$ for fixed $L = 5.2$ kbp (see Fig. 4 of Ref. [27]) and is in qualitative agreement with the picture outlined here. From $|\sigma| = 0$ to 0.02, R_g decreases: the chiral random coil states are more compact. Then, with supercoils, for $|\sigma| > 0.02$, R_g gradually increases again due to a combination of the slight increase of the superhelical axis length and the decreasing branch density. For larger L, the decrease in R_g as a function of $|\sigma|$ should slowly become more pronounced.

VI. DYNAMICS OF SUPERCOILED DNA AND INTRACHAIN REACTION KINETICS

Many biological processes involve the reaction of proteins with two (or more) sites on a DNA molecule [10,11,54]. For example, a viral DNA segment may be inserted into the host DNA and later excised [55]. In many cases, these reactions can only occur at special sites with specific base-pair sequence. Their rate is therefore limited by the time required to juxtapose the specific sites at which the integration or excision enzyme can work. It is of interest to estimate these rates, in particular how they depend on supercoiling, within the standard elastic model for DNA *in vivo*.

Below we review classical work for intrachain reaction of a "random-coil" polymer that describes the juxtaposition dynamics for unsupercoiled DNA [10,56]. We then generalize to supercoiled DNA in the three length regimes delineated in Sec. V. Supercoiling does not dramatically accelerate intramolecular reactions and in particular the "slithering" of the DNA molecule through the supercoil is rarely rate limiting. We finally describe two experiments that address these issues.

A. Unsupercoiled DNA

Unsupercoiled DNA undergoes intracoil relaxation via Zimm dynamics. Doi [56] has estimated that the characteristic time for first approach to a range δ (in the diffusion-limited case) for a Gaussian coil is of order

$$\tau_0 \approx 0.195 \left(\frac{b^3\eta}{k_BT}\right) N^{3/2} \ln \frac{Nb^2}{\delta^2}, \tag{39}$$

which for $b = 2A$ [32], $\eta = 0.01$ P, $k_BT = 4 \times 10^{-14}$ ergs, and $\delta = 1$ nm is about

$$\tau_0 \approx 10 \frac{\eta A^3}{k_BT} \left(\frac{L}{2A}\right)^{3/2} \left(1 + \frac{\ln L/2A}{9.2}\right). \tag{40}$$

For $L < 10^5$ nm ≈ 300 kbp we can ignore the logarithm and the reaction time is on the order of the longest Zimm time

$$\tau_0 \approx \frac{\eta A^3}{k_BT} \left(\frac{2L}{A}\right)^{3/2} \approx \frac{\eta R_g^3}{k_BT}. \tag{41}$$

The persistence length reorientation time is $\eta A^3/k_BT \approx 30 \times 10^{-6}$ sec. Berg [10] has arrived at a similar estimate for τ_0.

B. Plectonemically supercoiled DNA

If there are no branches on a plectoneme (i.e., for $L < \lambda \approx 1000$ nm or 3 kbp), intramolecule reactions between distant sites can proceed by bending of the supercoil, which can be treated as a Gaussian polymer of persistence length $2A$ and length $L/2$. Plugging the modified persistence and chain lengths into (41) we observe that the intrachain reaction time via bending is unchanged for such small chains.

For longer, branched, DNA molecules, but assuming $L < 25$ kbp, so that self-avoidance can be neglected, we can estimate the reorganization time by combining (36) with (41). In this range,

$$\tau_p \approx \frac{\eta A^3}{k_BT} \left(\frac{8\lambda L}{A^2}\right)^{3/4}. \tag{42}$$

We see that $\tau_p/\tau_0 = (2\lambda/L)^{3/4}$, indicating that interchain reactions are accelerated, but not by much, since for ≈ 8 branches or more the chain size again scales as $R_g \sim L^{1/2}$.

For $L > 25$ kbp, i.e., in the branched self-avoiding regime, combining (37) with (41) yields a reaction time

$$\tau_p \approx \frac{\eta A^3}{k_BT} \left(\frac{R}{2A}\right)^{3/5} \left(\frac{\lambda}{4A}\right)^{3/10} \left(\frac{2L}{A}\right)^{3/2}. \tag{43}$$

This scales with L just like τ_0; the relative factor is $\tau_p/\tau_0 = (\lambda R^2/[16A^3])^{3/10} \approx 0.35$ for $\lambda = 1000$ nm and $R = 8$ nm. So there is a possibility of a slight speedup as a result of plectoneme formation in this case as well.

C. Random slithering of supercoiled DNA does not speed up intramolecular reactions

The slithering or conveyer beltlike motion of DNA through a plectonemic supercoil is guaranteed to bring any two sites into the same supercoil. However, unless there is a motor to bias the process, the motion is diffusive and as such its characteristic time scales as L^3 as is typical for reptation processes in which a polymer slides along its track in a polymer melt [12].

To derive this time for supercoiled DNA, consider the hydrodynamic drag force between two rods each of length $L/2$ and hydrodynamic radius r_h a distance $2R$ apart, moving in opposite directions with speeds $\pm v$ in a fluid of viscosity η:

$$f_{\text{drag}} = \frac{2\pi\eta L v}{\ln(R/r_h)}. \tag{44}$$

The two pieces of rod represent the two pieces of DNA in the interwound plectoneme, each $L/2$ in length and separated by a distance of twice the plectonemic radius (we take $r_h = 4$ nm). The logarithmic flow fields of one rod are mutually cut off, leading to the $\ln(R/r_h)$ dependence.

The ratio of drag force to velocity gives the diffusion constant for the one-dimensional slithering motion of

$$\frac{k_BTv}{f_{\text{drag}}} = \frac{k_BT \ln(R/r_h)}{2\pi\eta L}, \tag{45}$$

which yields a time necessary to explore a length L by slithering diffusion of

$$\tau_s \approx \frac{2\pi\eta L^3}{k_BT \ln(R/r_h)}. \tag{46}$$

This is longer than τ_0 for $L > 2A(\ln[R/r_h]/2\pi)^{2/3}$, which always holds.

Several caveats should be noted before comparing these times with those of Sec. VI B or with experiment. First, supercoiling alone guarantees an *initial* reaction rate greater than $1/\tau_p$ or $1/\tau_s$ simply because the pairwise density of DNA is larger for distances less than R. Our estimates refer only to the time for a substantial fraction (e.g., 67%) of the molecules to react and then only when the reactive sites are a distance $\approx L/2$ apart on the DNA molecule. The slithering time in particular can be considerably enhanced if the two reactive sites are spaced by a distance $L_b \ll L$, which is small enough so that they will be both inside a clump of one or a few branches. Then one can imagine diffusing the entire clump in space (which happens rapidly) while slithering occurs just within a region of contour length L_b. The comparison of τ_s with τ_p is then based on L_b rather than L and is consequently less dramatic. However, if the plectoneme is linear, then even nearby sites *must* diffuse a distance $\sim L$ to the ends of the plectoneme in order to react.

Having thus cautioned the reader, we note that (46) yields nearly a minute for a 10 kbp plasmid and for R several times r_h. Slithering is further impeded if spontaneously curved sequences are present, which will tend to reside at the ends of branches or at branch points [29], acting as traps for the one-dimensional diffusion process. We are convinced that random slithering is not a rate-limiting process for reaction of two specific sites if they are more than a few kbp apart on a supercoiled plasmid of more than 10 kbp.

D. Experiments on intramolecule communication

Experiments to directly test the above conclusions are feasible, using proteins that interact with specific sequences on DNA. An example is the protein resolvase, two units of which bind to two *res* base-pair sequences along a DNA in order to carry out a recombination reaction (see Fig. 7). If the initial two sites are on the same DNA circle, then the recombination reaction results in a pair of catenated rings. This reaction can occur only when there are three crossings of a right-handed plectonemic supercoil between the two directly repeated *res* sites as shown in Fig. 7, which will require internal arrangement — most likely via slithering — of the DNA in a supercoil with many plectonemic turns [54].

Parker and Halford [11] have measured an upper bound of 0.1–0.5 sec for the time required to bring two sites separated by 1.1 kbp together (synapsis), on a 5 kbp supercoiled DNA. This time is considerably shorter than $\tau_s \approx 5$ sec predicted using the full plasmid length, but longer than $\tau_s \approx 5$ msec based on 1.1 kbp, or $\tau_p \approx 20$ msec using 5 kbp. All the caveats noted above regarding nonuniform reaction rates should be recalled. In fact, the plasmid length and site spacing in Ref. [11] are well chosen to put the reactive sites on the same branch, on which they may combine via bending and at the same time trap a small number of supercoils in between. Much more revealing, given the lack of an explicit time course for the reaction and the uncertainity in the prefactors in all our predictions, would be a study of how the rate depends on L for sites separated by a fixed, $\mathcal{O}(1)$ fraction of L. For a 30 kbp plasmid, we predict $\tau_p \approx 0.1$ sec and $\tau_s \approx 1000$ sec, leaving a large gap within which to verify the functional dependence on L.

A second site-specific recombination agent that might be suitable for studies of intramolecule communication is Int, which was discussed above (see Fig. 5). Somewhat like resolvase, Int carries out a recombination reaction at specific *att* sites on a single supercoiled circular DNA substrate [55]. However, Int does not require a specific number of supercoils to be between the sites. The reaction appears to require only the juxtaposition of the *att* sequences, which is a simpler process to model.

Int reaction product topology depends on the number of supercoils between the two *att* sites at the moment of the reaction, a property used by Boles *et al.* [8] to measure the number of superhelical turns in plasmids of known σ. In that study, it was proposed that there was no *a priori* dependence of the reaction rate on the number of supercoils between the two *att* sites: reactions are assumed to occur via "random collisions" of different plectonemic turns (see Fig. 4 of [8]) of the plectonemic axis. This is in accord with our conclusion that random coil fluctuations are the principal process by which

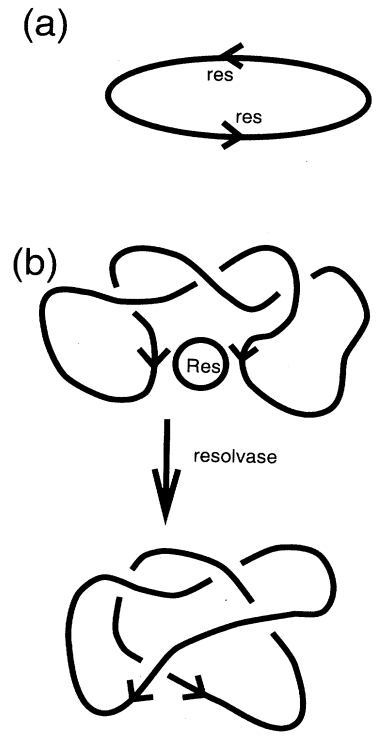

FIG. 7. Resolvase recombination of a DNA circle. (a) Unsupercoiled DNA ring; arrows show directly repeated *res* sequences. (b) The reaction requires three plectonemic crossings between the aligned *res* sites. (c) Two catenated rings are the product. This figure is adapted from Ref. [11].

distant-site juxtapositions occur.

However, Int studies may have something to say about slithering as well. If random slithering had been the dominant dynamical process in the Int experiments, an abundance of products in one topological state corresponding to juxtaposition of the two *att* sites across the same plectonemic turn would have been expected. This was not observed in experiments on supercoiled 9.4 kbp plasmids [55] with *att* sites separated by 1.5 kbp. Examination of the raw data indicates that the fraction of reactions that go to this specific topological state is *reduced* by supercoiling of the substrate (see Fig. 8 of [55]).

These experiments are therefore consistent with our thesis that slithering does not bring the *att* sites into synapsis as quickly as do random coil motions. This conclusion is supported by comparison of (41) with (46) using $L = 1.5$ kbp, giving $\tau_s/\tau_p \approx 100$. If the sites are on different branches, slithering will be even slower relative to bending at bringing the sites into synapsis.

VII. ENTROPIC ELASTICITY OF SINGLE DNA MOLECULES

Micromanipulation techniques for single DNA molecules in solution have recently been developed [57], making it possible to measure the force required to extend a single DNA molecule of, e.g., 100 kbp, from roughly 25% to nearly 100% of its full length. This measurement can be extended to nonzero linking number if the DNA is unnicked and a means is found to anchor both ends of both strands to the $\sim 3\mu$ beads which are the objects actually manipulated.

For low linking numbers ($|\sigma| \leq 0.01$), the force at given extension should be higher than, but generally follow, the $\sigma = 0$ case. For $|\sigma| \geq 0.02$, when the plectoneme state is preferred for a loop, the stretched DNA will partition into an extended solenoidal phase and plectonemic loop, with the plectonemic fraction decreasing with increasing extension. The zero-temperature version of this phenomenon is readily demonstrated with a rubber tube. Thermodynamically this experiment is analogous to phase coexistence where the extension and force are like volume and pressure and σ is a conserved quantitity that partitions between the two phases. This experiment should yield a wealth of information about the interplay of twisting and writhing at fixed linking number, as well as an accurate measure of the static twist elastic constant C.

A. Force law for a DNA molecule with $\sigma = 0$

For $\sigma = 0$, the twisting degrees of freedom do not affect the force law and the problem reduces to the calculation of the free energy of a persistent chain under traction, first discussed in detail by Fixman and Kovac [58]. The essential results are that for low extensions $z < L/2$, the force f is asymptotically linear as expected for a weakly biased random walk: $f = (3/2)(k_BT/A)z/L$. For extensions $z \approx L$, the force diverges as $f \approx (1/4)(k_BT/A)(1 - z/L)^{-2}$. In between, the force law may be computed numerically [58]. The crossover force k_BT/A follows from the fact that the persistence length A is the size of one degree of freedom for the unstretched chain. Using $A = 50$ nm and $T = 300$ K, $k_BT/A = 0.08$ pN. A useful but *approximate* interpolation between the low and high force limits is

$$\frac{fA}{k_BT} = [(1 - z/L)^{-2} - 1]/4 + z/L. \tag{47}$$

A fit to the experimental data definitely requires the exact force law and provides a very accurate measure of A and the length per bp under realistic solution conditions [59].

B. Force law for a DNA molecule with $\sigma \neq 0$

The plectoneme equation of state, i.e., $F_p(\sigma)$ obtained by minimization of (22), was calculated in Sec. IV and it remains to do the same for the solenoid, which is more involved since it depends on f as well as σ. With the free energies of the two "pure" phases in hand, we will determine the partitioning of σ and L between them so as to minimize the total free energy. Along the way, we will have to model the unbinding of the DNA since $|\sigma|$ concentrates in the plectoneme because of its lower free energy at high σ.

1. Stretched solenoidal supercoil

The starting point will be a regular helical coil of pitch P and radius R, around which we consider fluctuations. The energy for a helical supercoil being stretched in the z direction by a force f is

$$\frac{E[R,P,\mathbf{u}(s)]}{k_BT} = \int_0^L ds \left[\frac{A}{2}(\partial_s^2\mathbf{r})^2 - \frac{f}{k_BT}\hat{\mathbf{z}}\cdot\partial_s\mathbf{r}\right] + \frac{CL\Omega^2}{2}, \tag{48}$$

where $\Omega = \sigma\omega_0 \mp (1 - \sin\gamma)/\ell$ is the excess twist for a solenoidal structure, with upper and lower signs indicating right- and left-handed helices, respectively. The force enters as a Lagrange multiplier conjugate to the extension $\mathbf{r}(L) - \mathbf{r}(0)$ along the z axis. Writhe fluctuations have been dropped since we expect the force to set the correlation length scale and thereby the free energy (Appendix B).

The energy may be expanded in the same way as was done in the study of the supercoil (Appendix A): we use cylindrical coordinates (r, θ, z) and consider fluctuations $\mathbf{u}$ about a reference superhelix of pitch P and radius R, $\mathbf{r}(s) = R\hat{\mathbf{r}}(s) + s\sin\gamma\hat{\mathbf{z}} + \mathbf{u}(s)$. Expansion to quadratic order in Fourier components $\mathbf{u}_k \equiv \int ds \exp(iks/\ell)\mathbf{u}(s)$ gives

$$\frac{E}{k_BT} = \frac{AL\kappa^2}{2} + \frac{CL\Omega^2}{2} - \frac{f}{k_BT}L\sin\gamma + \frac{A}{2}\int \frac{dk}{2\pi\ell^5} u_{ik}^* \left(E_{ij} + \frac{f\ell^3}{k_BTAP}D_{ij}\right) u_{jk}, \tag{49}$$

where the matrix D is

$$D_{\theta\theta} = (k^2-1)^2, \quad D_{zz} = k^2(a^2k^2+a^2+1), \quad D_{\theta z} = D_{z\theta} = ak^2(k^2-1), \tag{50}$$

where $a \equiv P/R$. As before, $\kappa = R/[R^2+P^2]$ is the curvature of the reference superhelix of pitch P and radius R, $\sin\gamma = P/[R^2+P^2]^{1/2}$, and E_{ij} is the matrix obtained from bending fluctuations of a superhelix in Appendix A. We note that, in general, fluctuations will be reduced and this expansion approach will be valid when $f \gg k_BT/A$ or when the applied force substantially exceeds the characteristic entropic force.

The last of the nonfluctuating contributions and the matrix D_{ij} come from expansion of the force-extension term. Linear terms have been dropped, namely, u_r (its mean value is zero) and s derivatives of u_θ and u_z (reduced to boundary terms). The remaining quadratic term acts to reduce the z length.

The dimensionless combination $g = f\ell^2/(k_BTA\sin\gamma)$ will be used below. For the moment we focus on the fluctuation contribution to the free energy

$$\frac{\Delta F}{k_BT} = -\sum_{k=\pm 2\pi n\ell/L} \ln\left[\int du_{\theta k}\int du_{zk} \times \exp\left(-\frac{A}{2\ell^4 L}u^*_{ik}\left[E_{ij}+gD_{ij}\right]u_{jk}\right)\right] - \frac{\Delta F_0}{k_BT}. \tag{51}$$

We will fix the unmeasurable constant ΔF_0 by requiring ΔF to vanish for $g=0$; therefore

$$\frac{\Delta F}{k_BTL} = \int \frac{dk}{4\pi\ell}\ln\left(\frac{\det[E+gD]}{\det[E]}\right) = \frac{I(\sin\gamma, g)}{\ell}, \tag{52}$$

where the function I is (after use of the explicit formulas for D and E and some algebra)

$$I(s,g) = \int \frac{dk}{4\pi}\ln\left(\frac{k^4-(3s^2-1-2g)k^2+s^2+[1+s^2]g+g^2}{k^4-(3s^2-1)k^2+s^2}\right) = \left[\frac{1}{2}(g+1)^{1/2}(g+s^2)^{1/2} - \frac{3}{4}s^2 + \frac{1}{4} + \frac{g}{2}\right]^{1/2} - \left[\frac{1}{2}s - \frac{3}{4}s^2 + \frac{1}{4}\right]^{1/2}. \tag{53}$$

If $\sin\gamma = 1$ there is no superhelicity and we recover results for a straight polymer: $I(1,g) = g^{1/2}$ and ℓ disappears from the result

$$\frac{\Delta F}{k_BTL} = \left(\frac{f}{k_BTA}\right)^{1/2}, \tag{54}$$

which is precisely the divergence in the free energy for $fA/k_BT \gg 1$ encountered in the theory of the stretched wormlike chain [58]. This limit is also realized for large g.

The solenoidal free energy is obtained in analogy to Sec. IV by minimizing the sum of the constant $u=0$ terms in (49) and the fluctuation term (52) with respect to pitch and radius or $\sin\gamma$ and ℓ,

$$\frac{F_s(\sigma,f)}{k_BTL} = \min_{\ell,\sin\gamma}\left[\frac{A\kappa^2}{2} + \frac{C}{2}\left(\sigma\omega_0 \mp \frac{1-\sin\gamma}{\ell}\right)^2 - f\sin\gamma/k_BT + \frac{I(\sin\gamma,g)}{\ell}\right]. \tag{55}$$

The extension is

$$z = \hat{\mathbf{z}}\cdot[\mathbf{r}(L)-\mathbf{r}(0)] = -\frac{\partial F_s}{\partial f}. \tag{56}$$

For the uncoiled case $\sin\gamma = 1$ we obtain the stress-strain curve

$$f = \frac{k_BT}{4A(1-z/L)^2}, \tag{57}$$

in agreement with (47) for $z \to L$. A comparison to the exact straight-chain result from the wormlike chain model under traction shows that this formula is accurate for $z/L > 1/2$: this may be taken as a criterion for when our F_s may be trusted.

2. *Partition of a stretched chain into plectonemic and solenoidal regions*

Now we put together the plectonemic free energy per length $F_p(\sigma_p)/(k_BTL)$, which is a function of the linking number contained in the plectoneme, and the free energy per length of the extended solenoid $F_s(\sigma_s, f)$ to compute the properties of a stretched piece of twisted DNA. We suppose that a fraction x_s of the extended supercoil is solenoidal, while the remainder is plectonemic. If the total excess linking number is σ, we know that it must be partitioned into linking contributions σ_p on the plectoneme and σ_s on the solenoid as

$$\sigma = x_s\sigma_s + (1-x_s)\sigma_p, \tag{58}$$

allowing σ_p to be eliminated in favor of x_s and σ_s. The supercoil free energy per length is simply the sum of appropriately weighted components, with free parameters again determined via minimization

$$\frac{F(\sigma,f)}{k_BTL} = \min_{x_s,\sigma_s}\left[x_s\frac{F_s(\sigma_s,f)}{k_BTL} + (1-x_s)\frac{F_p(\sigma_p)}{k_BTL}\right]. \tag{59}$$

The total extension is simply $z = -\partial F/\partial f$.

3. Results

The extension versus force f, shown in Fig. 8, was found by minimizing (59) numerically, using the plectoneme and solenoid free energies (22) and (55). In Figs. 8(a) and 8(b), the dashed $\sigma = 0$ curve is the exact result for the wormlike chain under traction [58], which quantitatively describes experiments with $\sigma = 0$ [59]. The force is shown in units of k_BT/nm ($1k_BT$/nm $\approx$ 4 pN); the crossover from the low-f to the high-f regime for $\sigma = 0$ is seen to be near $k_BT/A = 0.02k_BT$/nm. As σ increases, we find that more force is needed to obtain a given extension.

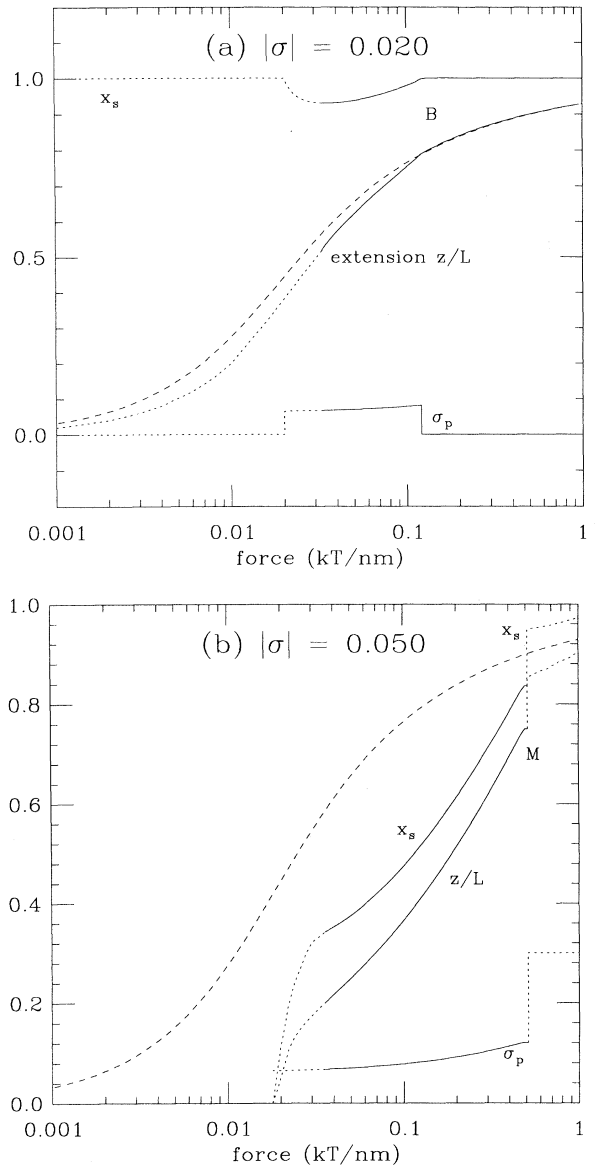

FIG. 8. Extension versus force for DNA with fixed linking number (note 1 k_BT/nm $\approx 4\times10^{-12}$N). The $\sigma = 0$ calculation (dashed curve) is exact while the other curves are calculated in the large-force limit; that Gaussian calculation is in error by $\geq 5\%$ for extensions $z/L < 0.5$ and 0.25 for $|\sigma| = 0.02$ and 0.05, respectively, and below these limits expected behaviors are dotted. A plectonemic bubble appears with decreasing force at point B for $|\sigma| = 0.02$. For $|\sigma| = 0.05$ the concentration of link in the plectonemic region causes the DNA to unbind or melt at point M as force increases; results beyond M are dotted, since they depend on poorly known details of melted DNA.

For $|\sigma| = 0.02$ [Fig. 8(a)], a large force $f > 0.1k_BT$/nm eliminates all net writhe, the link is forced entirely into twist, and the extension is identical to that of a $\sigma = 0$ random coil. As f decreases to $0.1k_BT$/nm, a small plectonemic "bubble" appears in coexistence with the extended solenoid [where $x_s < 1$ in Fig. 8(a)]. This bubble has $|\sigma_p| \sim 0.08$, notably larger than $|\sigma|$ because of the lower free energy of the plectoneme for given σ. This bubble grows to be $\sim 8\%$ of L for a fractional extension of 0.5; for extensions less than this the calculation is unreliable. We expect the plectoneme phase to vanish entirely as $f \to 0$ because $|\sigma|$ is below the transition point found in Sec. IV D, and we expect the extension to remain similar to the unsupercoiled case.

For larger $|\sigma|$, for example, 0.05 [Fig. 8(b)], where the $f = 0$ state is plectonemic, a finite force (equivalent to a free energy per length) must be exerted to have any extension at all. As f increases for $\sigma = 0.05$, there is again a tendency to concentrate σ in the plectoneme phase, but now $|\sigma_p|$ can exceed 0.12, which we take somewhat arbitrarily to be the point where the double helix undergoes a structural transition [note the discontinuity at $f \approx 0.4k_BT$/nm in Fig. 8(b)]. Our calculation works to lower extensions than for $|\sigma| = 0.02$ since there is sufficient force on the solenoid to justify a Gaussian approximation. For $|\sigma| = 0.065$ and 0.075 we predict a limiting force of 0.02 and 0.08 k_BT/nm at zero extension whose experimental determination would be a sensitive test of our theory.

The model that produced the jump at point M of Fig. 8(b) supposes an alternative DNA secondary structure with $|\sigma| = 0.3$ lying $\approx 2k_BT$/nm in energy higher than the B form. Equivalently, we replace the actual $F_p(\sigma)$ for $\sigma \geq 0.12$ by the tangent at that point out to $\sigma = 0.3$ and infinity beyond.

VIII. EFFECT OF ATTRACTIVE DNA-DNA INTERACTIONS ON SUPERCOILING

The cryo-EM experiments [21] suggest that there are attractive interactions that can collapse plectonemic superhelices into a tightly interwound configuration. In this section we propose a simple theoretical model for this phenomenon.

A convenient parametrization of a short-range attraction is obtained by simple addition of an attractive Gaussian potential with a range $r_0 = 1.2$ nm (the DNA radius) to the screened Coulomb interaction (2). For two DNA molecules spaced by $2R$ we have the energy per length

$$w(R)/k_BT = \ell_B\nu^2K_0(2\kappa R) - ue^{-R^2/r_0^2}. \qquad (60)$$

The Gaussian decays faster than, and does not affect, the exponential screened Coulomb interaction; at short distances, it is finite and does not affect the divergent repulsive Coulomb core.

The pseudopotential u is the k_BT per length introduced by the attractive interaction and the scale at which the repulsion starts to be overcome by attraction in this model is $u \approx 2$ nm^{-1}. When added to the plectoneme free energy (22), a new state appears that is a "collapsed" plectoneme with the double helices separated by a distance of somewhat larger than $2r_0$, corresponding to the state of affairs observed in the cryo-EM experiments.

Figure 9 illustrates how this collapse works, showing plectoneme radius R in nanometers vs added linking number σ. The dashed line shows the "swollen plectoneme" result of Fig. 3 with no attractive component to DNA-DNA interaction ($u = 0$), while the solid curves show R for $u = 3$ nm^{-1}. For $|\sigma| < 0.05$, $R > 4$ nm and there is little effect of the attraction since at these ranges the short-ranged Gaussian interaction is dwarfed by the power-law entropic interaction.

However, for larger $|\sigma|$, R begins to be depressed by the attraction and at $|\sigma| = 0.064$ a new, collapsed plectoneme state appears (lower solid curve, $R \approx 2$ nm). This new state is lower in free energy than the swollen plectoneme state for $|\sigma| > 0.071$; at $|\sigma| > 0.075$ the swollen state ceases to even be metastable. The collapsed state stable at high $|\sigma|$ is characterized by a nearly constant value of R determined primarily by a balance of the attractive and electrostatic interactions. The location of the swollen-collapsed transition region can be moved to lower $|\sigma|$ if u is increased. Further increase of u eliminates the swollen plectoneme state entirely. Coexisting open and collapsed plectonemic regions on the same plasmid have been reported in experiments of Dubochet *et al.* [21] and are consistent with the "overlap" of the collapsed and swollen states apparent in Fig. 9.

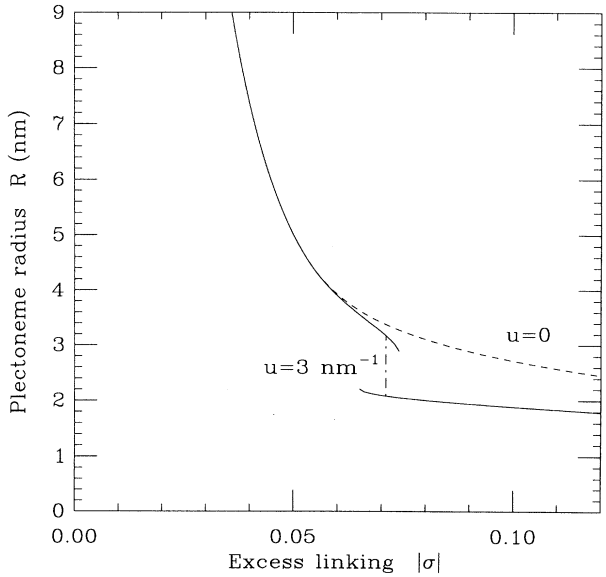

FIG. 9. Plectoneme radius R in nm vs added linking number σ. The dashed line shows the result of Fig. 3 with no attractive component to the DNA-DNA interaction ($u = 0$). The solid curves show R for moderately strong attraction ($u = 3$ nm^{-1}); for $|\sigma| < 0.05$, $R > 4$ nm and there is little effect of the attraction, but for larger $|\sigma|$ there occurs a transition to a "collapsed" plectoneme state with $R \approx 2$ nm.

This calculation indicates that it is possible for attractive interactions to be too weak to affect the molecule conformations for small $|\sigma|$, yet strong enough to cause the qualitative change in conformation of plectonemic collapse for larger σ. As suggested by Dubochet *et al.* [21], the entropy of the large conformational fluctuations enjoyed at small $|\sigma|$ overwhelms the enthalpic attractive interaction, but as conformational fluctuations and the entropy is reduced (as free energy is increased) at larger $|\sigma|$, a small attraction can induce collapse.

IX. CONCLUSION

We have described the supercoiling, or buckling, of a DNA molecule under twisting strain. The prototypic case considered is that of a circular DNA molecule with the linking number of the double helix changed from its elastic equilibrium value. For supercoiling to occur, the linking number must be changed by a macroscopic amount (about 2% of the total molecule linking number) away from its equilibrium value; for smaller linking numbers an open random-coil conformation occurs. Precisely this behavior is observed in experiments [8] and in large-scale Monte Carlo calculations [25–28]. Most plasmids (small circular DNA molecules of lengths in the range 1–10 kbp found in bacteria and yeast) have linking numbers that are about 5% away from elastic equilibrium and therefore are supercoiled.

Elastic energy and fluctuation entropy compete to determine the structure of supercoiled DNA molecules. Fluctutation entropy acts to swell the supercoil diameter far beyond the range of direct physiochemical interactions (e.g., electrostatic interactions with *in vivo* salt concentrations). In addition, fluctuations generate about one branch point along the plectonemic axis every 1 or 2 kbp. These effects have been observed experimentally and in computer simulations and cannot be understood without consideration of thermal fluctuations.

Via minor modification of our basic model we have shown that supercoil collapse may be driven by weak DNA-DNA attractions. This may be relevant to recent cryo-EM experiments [21]. The physical mechanism of such attractions in room-temperature solution is open and deserves experimental study.

We have also estimated time scales for intramolecular reactions on unsupercoiled and supercoiled DNA molecules in response to recent experiments [11]. Generally speaking, such reactions will require a time on the order of the relaxation time of the chain conformation. Supercoiling somewhat reduces the size of a plasmid and can slightly accelerate such reactions. We have argued that random "slithering" or "reptation" processes do not limit the rate at which distant sites on a supercoiled molecule are juxtaposed. Intra-DNA recombination reactions provide unique experimental systems for study of polymer dynamics and should be of interest to the polymer science community as well as to biochemists. Our initial work indicates that molecular dynamics of a single supercoiled DNA of a few kilobases involves a tremendously wide range of time scales reminiscent of highly entangled polymers.

Recent experiments manipulating single DNA molecules [57] have allowed precise measurement of the bending elasticity of DNA [59]. The obvious next step that we have discussed in some detail is precision measurement of the elasticity of twisted DNA. The type of biochemical linkage commonly used in such experiments (e.g., biotin-streptavidin) does not constrain twist. Use of fasteners that anchor both strands would allow a precise study of the very rich thermodynamics of twisted DNA.

Enzymes that replicate or translate DNA cannnot rotate around the double helix as they "read" the base pairs at rates up to 10^3 bp/sec. Thus the DNA is overwound ahead of the enzyme and underwound behind it and this twist can diffuse out the ends of the molecule if they are free [60]. More typically, because of constraint of the ends, this twist is relaxed by topology-changing enzymes, of which many must act in series because of their lower processivity. This coupled system of enzymes suggests interesting dynamical-structural questions such as kinetically induced supercoiling that could be addressed by the methods of this paper.

Our phenomenological scaling results apply to any polymer whose bending and twisting elastic constants are comparable. For instance, we can describe the supercoiling of chromatin fiber as easily as pure DNA. A more challenging application would be to two catenated double-stranded DNA loops [61]. The effective twist and bend elastic constants for the linked molecules, thought of as a unit, themselves would have to be calculated from fluctuation effects before supercoiling of the entire loop could be considered.

Note added in proof. With a screening length $\lambda_D \sim 3$ nm appropriate for 10 mM NaCl solution, the DNA unbinding transition reported in Fig. 8(b) for physiological salt concentration (140 mM NaCl), does not occur. Hence this transition is readily tunable, so one may speculate that a cell could achieve the same effect with DNA binding proteins, and thereby regulate the initiation of replication or transcription.

ACKNOWLEDGMENTS

We gratefully acknowledge helpful discussions with C. Bustamante, N. R. Cozzarelli, M. Frank-Kamenetskii, P. Model, M. Schmid, A. Stasiak, D. Smith, S. Smith, D. Sumners, and A. Vologodskii. This research was supported by the National Science Foundation under Grant No. DMR 9012974 and by the MRL Program of the NSF under Grant No. DMR-9121654. J.M. gratefully acknowleges support at RU from the Meyer Foundation.

APPENDIX A: CALCULATION OF THE DNA-DNA ENTROPIC INTERACTION

In this appendix we present a detailed calculation of the effective entropic interaction brought about by confinement of a DNA into a superhelix. We first analyze the normal modes of a superhelix with fixed average R and P; we then compute the free-energy change imparted by a constraint on the fluctuation of those modes. The last subsection discusses the self-consistency of the free-energy calculation.

1. Superhelix normal modes

We adopt helical-cylindrical coordinates (r, θ, z) with the z axis along the unperturbed superhelix axis: The supercoil is described as

$$\mathbf{r}(s) = \mathbf{r}_0 + \mathbf{u}(s), \tag{A1}$$

where $\mathbf{r}_0 = s\hat{\mathbf{z}}\sin\gamma + R\hat{\mathbf{r}}(s)$ is the reference superhelix parametrized by R and $\sin\gamma$, s is arc length along the DNA backbone, and $\mathbf{u}$ is a vector function of s that describes the fluctuations about the reference superhelix. The radial unit vector varies with s: $\hat{\mathbf{r}}(s) = \hat{\mathbf{x}}\cos(s/\ell) \pm \hat{\mathbf{y}}\sin(s/\ell)$, where the upper and lower signs generate right- and left-handed superhelices. The angular unit vector $\hat{\theta} = \ell\partial_s\hat{\mathbf{r}}$. It will be useful to define the unit reference tangent vector $\hat{\mathbf{t}}_0 = \partial_s\mathbf{r}_0$.

The curvature squared may be written as

$$\kappa^2 = \frac{R^2}{\ell^4} + (\partial_s^2\mathbf{u})^2 - 2\frac{R}{\ell^2}\hat{\mathbf{r}}\cdot\partial_s^2\mathbf{u}. \tag{A2}$$

The first term is just the static curvature; the second is curvature fluctuations. The third term, the cross term, may be ignored if we note that it reduces to

$$\hat{\mathbf{r}}\cdot\partial_s^2\mathbf{u} = \partial_s^2 u_r - \frac{2}{\ell}\partial_s u_\theta - \frac{1}{\ell^2}u_r. \tag{A3}$$

The derivatives may be integrated away; the nonderivative term may be ignored as we want an ensemble where u_r is constrained to have a zero expectation value. Imposing this one constraint is sufficient to render the fluctuation energy positive definite, which is necessary for the two-step minimization process envisioned in Sec. IV to be meaningful. Algebra leads to

$$\begin{aligned}\partial_s^2\mathbf{u} = \hat{\mathbf{r}}&\left(\partial_s^2 u_r - \frac{2\partial_s u_\theta}{\ell} - \frac{u_r}{\ell^2}\right)\\ &+\hat{\theta}\left(\partial_s^2 u_\theta + \frac{2\partial_s u_r}{\ell} - \frac{u_\theta}{\ell^2}\right) + \hat{\mathbf{z}}\partial_s^2 u_z.\end{aligned} \tag{A4}$$

The constraint $|\partial_s\mathbf{r}| = 1$, when written out in terms of (A1), may be reexpressed as

$$u_r = -\ell\partial_s\left[u_\theta + a u_z\right] - \ell(\partial_s\mathbf{r})^2/(2R), \tag{A5}$$

where $a = \tan\gamma$. Linear order is sufficient since all terms in the curvature energy (A2) are quadratic. It is convenient to eliminate u_r and to work with u_θ and u_z as the independent degrees of freedom, as it may be shown that the original path integration measure $\int D\hat{\mathbf{t}}$ may be replaced by $\int Du_\theta Du_z$ at Gaussian order.

In terms of Fourier transforms $u_{i,k} \equiv \int ds\exp(iks/\ell)u_i$ for $i = \theta, z$ and dimensionless wave number k the curvature energy is

$$\frac{\Delta E}{k_B T} = \frac{A}{2}\int\frac{dk}{2\pi\ell^5}\sum_{i,j\in\{\theta,z\}} u_{i,k}^* E_{ij} u_{j,k} + O(u^3), \tag{A6}$$

where the dimensionless matrix E has entries

$$\begin{aligned}E_{\theta\theta} &= (k^2+1)(k^2-1)^2,\\ E_{zz} &= k^4 + a^2k^2(k^4+6k^2+1),\\ E_{\theta z} = E_{z\theta} &= ak^2(k^2-1)(k^2+3).\end{aligned} \tag{A7}$$

Diagonalization of E yields two nondegenerate nonnegative eigenvalues

$$\lambda_\pm = \frac{1}{2}\left[(E_{\theta\theta}+E_{zz}) \pm \sqrt{(E_{\theta\theta}-E_{zz})^2+4E_{\theta z}^2}\right]. \quad \text{(A8)}$$

The normalized eigenvectors are

$$\hat{\mathbf{e}}_+ = \frac{1}{\sqrt{E_{\theta z}^2+(\lambda^+-E_{\theta\theta})^2}}\begin{pmatrix} E_{\theta z} \\ \lambda_+ - E_{\theta\theta}\end{pmatrix},$$
$$\hat{\mathbf{e}}_- = \frac{1}{\sqrt{E_{\theta z}^2+(\lambda^+-E_{\theta\theta})^2}}\begin{pmatrix} E_{\theta\theta}-\lambda_+ \\ E_{\theta z}\end{pmatrix}. \quad \text{(A9)}$$

For $k \to 0$, $\lambda_+ \to 1$ and $\lambda_- \to 0$; in this limit the eigenvectors are $\mathbf{e}_+ = \hat{\theta}$ and $\mathbf{e}_- = \hat{\mathbf{z}}$. The + mode is massive and corresponds to a displacement along the θ direction, which requires buckling of the polymer. The − (low-energy) mode has a zero at $k=0$ due to z-translational invariance; for small k it grows as $\lambda_- = a^2k^2$.

At $k=1$, $\lambda_+ = 1+8a^2$, but λ_- again has a zero. This zero (along with the one at $k=-1$) reflects translational invariance in the x-y plane. The low-energy mode behaves as $\lambda_- \propto (k\mp 1)^2$ near $k=\pm 1$. The eigenvectors at this point are $\mathbf{e}_+ = \hat{\mathbf{z}}$ and $\mathbf{e}_- = \hat{\theta}$.

At larger k, λ_+ continues to be of order unity until about $k=1$, at which time it starts to rapidly increase, asymptotically growing as

$$\lambda_+ = (1+a^2)k^6 + (6a^2-1)k^4 + O(k^2). \quad \text{(A10)}$$

For large k,

$$\mathbf{e}_+ = \left[\frac{1}{(1+a^2)^{1/2}} - \frac{4a^2}{(1+a^2)^{3/2}}k^{-2}\right]\hat{\theta} + \left[\frac{a}{(1+a^2)^{1/2}} + \frac{4a}{(1+a^2)^{3/2}}k^{-2}\right]\hat{\mathbf{z}} + O(k^{-4}). \quad \text{(A11)}$$

The low-energy mode increases less quickly beyond $k=1$, growing as

$$\lambda_- = k^4 - (10a^2)(1+a^2)^{-1}k^2 + O(1). \quad \text{(A12)}$$

Its eigenvector is

$$\mathbf{e}_- = \left[-\frac{a}{(1+a^2)^{1/2}} - \frac{4a}{(1+a^2)^{3/2}}k^{-2}\right]\hat{\theta} + \left[\frac{1}{(1+a^2)^{1/2}} - \frac{4a^2}{(1+a^2)^{3/2}}k^{-2}\right]\hat{\mathbf{z}} + O(k^{-4}). \quad \text{(A13)}$$

The low-energy mode spectrum is divided by the zero modes at $k=\pm 1$. For $|k|<\pm 1$, we have a wavelength larger than one helix spacing: although of importance for the global superhelix axis, these fluctuations will not be responsible for the superhelix colliding with itself at short length scales. The modes that will cause this are those with $|k|>\pm 1$.

2. Free energy of constrained fluctuations

We calculate the free energy of a superhelical configuration with fixed R and P: we anticipate a large free-energy cost if either R or P tends to zero. The fluctuations must be controlled using cutoffs, which we insert as "masses" $m_\pm$ in the eigenvalues

$$\lambda_+(m_+) \equiv (1+a^2)k^6 + (6a^2-1)k^4 + m_+^4(1+a^2)k^2 + O(1), \quad \text{(A14)}$$
$$\lambda_-(m_-) \equiv k^4 - 10a^2(1+a^2)^{-1}k^2 + m_-^4 + O(k^{-2}).$$

The masses are pseudopotentials whose strength will be self-consistently determined from the requirement that the fluctuations be controlled. The change in free energy due to the masses is easily computed

$$\frac{\Delta F}{Lk_BT} = \int_{-\infty}^{\infty}\frac{dk}{2\pi}\left[\ln\frac{\lambda_+(m_+)}{\lambda_+(0)} + \ln\frac{\lambda_-(m_-)}{\lambda_-(0)}\right] \quad \text{(A15)}$$
$$\approx \begin{cases}\sqrt{2}(m_+ + m_-)/\ell, & m^\pm \to \infty \\ (c_+m_+^4 + c_-m_-^2)/\ell, & m^\pm \to 0, c_\pm \approx 1.\end{cases}$$

Interpreting the masses as inverse correlation lengths (in units of ℓ), we see just the result that we expect for large $m_\pm$: of order k_BT per correlation length in confinement energy. As the masses go to zero, the free energy vanishes faster than linearly in $m_\pm$.

In order to set the masses, we compute the rms fluctuations in the r and z directions over a distance of one superhelix repeat of molecule length $2\pi\ell$:

$$\langle[u_i(s)-u_i(s+2\pi\ell)]^2\rangle = \int_{-\infty}^{\infty}\frac{dk}{2\pi\ell}2(1-\cos 2\pi k)\,\langle u_{ik}^* u_{ik}\rangle \quad \text{(A16)}$$

for $i=r$ and z. The necessary correlators are

$$\langle u_{ik}^* u_{jk}\rangle = \frac{\ell^4}{A}\left[\frac{(\hat{\mathbf{e}}_+\cdot\hat{\mathbf{i}})(\hat{\mathbf{e}}_+\cdot\hat{\mathbf{j}})}{\lambda_+} + \frac{(\hat{\mathbf{e}}_-\cdot\hat{\mathbf{i}})(\hat{\mathbf{e}}_-\cdot\hat{\mathbf{j}})}{\lambda_-}\right] \quad \text{(A17)}$$

for $i=\theta$ and z. At large k, these behave as

$$\langle u_{\theta k}^* u_{\theta k}\rangle \approx \frac{\ell^4}{A}\left[\frac{a^2}{(1+a^2)k^4} + \frac{1+8a^2+10a^4}{(1+a^2)^2k^6}\right],$$
$$\langle u_{zk}^* u_{zk}\rangle \approx \frac{\ell^4}{A}\left[\frac{1}{(1+a^2)k^4} + \frac{3a^2}{(1+a^2)^2k^6}\right], \quad \text{(A18)}$$
$$\langle u_{\theta k}^* u_{zk}\rangle \approx \frac{\ell^4}{A}\left[-\frac{a}{(1+a^2)k^4} - \frac{3a(1+2a^2)}{(1+a^2)^2k^6}\right].$$

The rr correlator is

$$\langle u_{rk}^* u_{rk}\rangle = k^2\left[\langle u_{\theta k}^* u_{\theta k}\rangle + a^2\langle u_{zk}^* u_{zk}\rangle + 2a\langle u_{\theta k}^* u_{zk}\rangle\right] = \frac{k^2\ell^4}{A}\left(\frac{\left[\mathbf{e}_+\cdot(\hat{\theta}+a\hat{\mathbf{z}})\right]^2}{\lambda_+} + \frac{\left[\mathbf{e}_-\cdot(\hat{\theta}+a\hat{\mathbf{z}})\right]^2}{\lambda_-}\right) \quad \text{(A19)}$$

and behaves at large k as

$$\langle u_{rk}^* u_{rk}\rangle \approx \frac{\ell^4}{A}\left[\frac{1}{k^4} + \frac{1+10a^2}{(1+a^2)k^6}\right]. \quad \text{(A20)}$$

As expected, the dominant term is identical to what one

would have for a straight filament.

The notation for the correlators is $\langle u_k u_{k'} \rangle \equiv 2\pi\ell\delta(k+k')\langle u_k^* u_k \rangle$, explaining the (length)^3 dimensions of the on-shell correlators. As usual, we use the relation $L = 2\pi\ell\delta(k=0)$ to convert our results from infinite to finite L.

The real-space correlators are not sensitive to the symmetry-related zero modes. The term $1-\cos 2\pi k$ has double zeros at $k=0$ and $k=1$, which cancel the corresponding double zeros of λ_-.

Suppose that pitch P tends to zero. Then we will have the constraint

$$\begin{aligned}\pi^2 P^2 &= \langle [u_z(s) - u_z(s+2\pi\ell)]^2 \rangle \\ &= \frac{\ell^3}{A}\int \frac{dk}{2\pi} 2(1-\cos 2\pi k)\left[\frac{1/(1+a^2)}{m_-^4+k^4} + \frac{a^2/(1+a^2)}{(1+a^2)k^2(m_+^4+k^4)} + \cdots\right] \\ &= \frac{\ell^3}{A}\left[\frac{2^{-3/2}}{(1+a^2)m_-^3} + \frac{a^2}{(1+a^2)^2 m_+^5}\int \frac{dk}{2\pi}\frac{2(1-\cos 2\pi m_+ k)}{k^2(1+k^4)} + \cdots\right].\end{aligned} \tag{A21}$$

The last integral ends up being proportional to m_+^{-4}. If R is finite and P is reduced to zero, the m_- term dominates this expression (it turns out that $m_+ \approx m_-^{4/5}$) and

$$m_- = \left(\frac{2^{-3/2}\ell^3}{(1+a^2)\pi^2 A P^2}\right)^{1/3}, \tag{A22}$$

where we have neglected the order-unity constant in the last term. The free energy is dominated by m_-, although m_+ also diverges as $P \to 0$ because the constraint on the z fluctuations cuts off both modes. Using (A15),

$$\frac{\Delta F}{k_B T L} = \frac{1}{(1+a^2)^{1/3} A^{1/3} (\pi P)^{2/3}}. \tag{A23}$$

Now we consider the case where the superhelix radius R tends to zero. We require the correlator

$$\begin{aligned}R^2 &= \langle [u_r(s) - u_r(s+2\pi\ell)]^2 \rangle \\ &= \frac{\ell^3}{A}\int \frac{dk}{2\pi} 2(1-\cos 2\pi k)k^2 \\ &\quad \times \left[\frac{1}{k^2(k^4+m_+^4)} + \frac{64a^2/(1+a^2)}{k^4(k^4+m_-^4)} + \cdots\right],\end{aligned} \tag{A24}$$

where in the second term the k^{-4} appears because of a cancellation of constant terms that has to occur in order to make the correlation function controlled by the $k^4 + m_+^4$ denominator so finally

$$R^2 = \frac{\ell^3}{A}\left(\frac{2^{-3/2}}{m_+^3} + \frac{O(1)a^2}{(1+a^2)m_-^4}\right). \tag{A25}$$

The case $R \to 0$ is therefore roughly the reverse of the situation when $P \to 0$ in that the roles of m_+ and m_- are exchanged. Thus (A25) implies

$$m_+ = \left(\frac{2^{-3/2}\ell^3}{AR^2}\right)^{1/3} \gg m_- \approx m_+^{4/5}. \tag{A26}$$

The free energy is

$$\frac{\Delta F}{k_B T L} = \frac{1}{A^{1/3} R^{2/3}}. \tag{A27}$$

If both R and P go to zero at about the same rate, R determines m_+ and P determines m_- through the relations derived above. The net free energy is just the sum of (A23) and (A27).

When the masses go to zero, the fact that we use a differenced correlator suppresses the symmetry-induced singularities. The maximum values of the correlators are

$$\langle [u_i(s) - u_i(s+2\pi\ell)]^2 \rangle_{m_i=0} \approx \ell^3/A \tag{A28}$$

for $i,j = r$ and z. Thus, when R^2 or $\pi^2 P^2$ approach ℓ^3/A, the masses very quickly go to zero. As we do not want to constrain modes with wavelength longer than a superhelix repeat (the writhe is insensitive to long-wavelength distortions of the superhelix), the confinement free energy is limited to that amount that can be pulled out of modes with $k > 1$.

A potential that takes into account all of these behaviors is

$$\begin{aligned}\frac{\Delta F}{k_B T L} = \frac{1}{A^{1/3}}\Bigg(&\frac{\gamma_p}{(1+a^2)^{1/3}(\pi P)^{2/3}} \\ &\times \frac{2}{1+\exp[\lambda_p \pi^2 P^2 A/\ell^3]} \\ &+ \frac{\gamma_r}{R^{2/3}}\frac{2}{1+\exp[\lambda_r R^2 A/\ell^3]}\Bigg).\end{aligned} \tag{A29}$$

We have inserted order-unity constants λ_r and λ_p that control exactly where the confinement free energy falls to zero. Also, we include order-unity prefactors γ_r and γ_p to take into account that there is some uncertainty in the prefactors of the power-law divergences. We have checked that changing the exact values of these parameters does not change any of the scaling behaviors. The pure power laws may be used without any qualitative change in the results of the theory [9]:

$$\frac{\Delta F}{k_B T L} = \frac{1}{A^{1/3}(\pi P)^{2/3}} + \frac{1}{A^{1/3} R^{2/3}}. \tag{A30}$$

These $-2/3$-law divergences could have been guessed using the naive scaling argument of Sec. IV. They are simply due to the short-distance k^4 behavior of the bending Hamiltonian and this appendix shows how the superhelical DNA conformation is superfluous.

3. Self-consistency for $R \to 0$ and $P \to 0$

Above it was argued that the constraint on the fluctuation amplitude sets the value of one of the masses $m_\pm$. However, one might ask how the second of the masses is set: this is done by free-energy minimization. Here we show that this second mass leads only to a subleading contribution to the fluctuation free energy when either R or P is reduced to zero.

The two constraints that pitch and radius be large compared to z and r fluctuations, respectively, are

$$AP^2/\ell^3 \geq m_-^{-3} + m_+^{-4}, \qquad \text{(A31)}$$
$$AR^2/\ell^3 \geq m_-^{-4} + m_+^{-3},$$

where order-unity prefactors have been dropped. The fluctuation free energy per has the form

$$\frac{\Delta F}{k_B T L} = (m_+ + m_-)/\ell. \qquad \text{(A32)}$$

Considering the case where $R \to 0$ (for which m_+ was supposed to be determined by the R constraint) we have a fluctuation free energy

$$\frac{\Delta F}{k_B T L} = m_+ + (AR^2/\ell^3 - m_+^{-3})^{-1/4}, \qquad \text{(A33)}$$

which when minimized with respect to m_+ gives

$$m_- \approx m_+^{4/5} \qquad \text{(A34)}$$

or $m_- \ll m_+$. Going back to R^2 we find

$$AR^2/\ell^3 \approx m_+^{-3} + m_+^{-16/5} \qquad \text{(A35)}$$

and we see that the contribution of m_- (the latter term) does not change the leading scaling. The last requirement is that the constraint on pitch is not violated by the solution: this is $AP^2/\ell^3 \geq m_+^{-12/5} + m_+^{-4}$.

When $P \to 0$, the roles of m_+ and m_- are reversed. The same procedure shows that $m_+ \approx m_-^{4/5} \ll m_-$: again the second mass makes a small correction to the free energy. The condition on radius required for self-consistency in this limit is

$$AR^2/l^3 \geq m_-^{-12/5} + m_-^{-4}. \qquad \text{(A36)}$$

APPENDIX B: WRITHE FLUCTUATIONS

The fluctuation of writhe provides information about two effects. One is the estimation of the contibution of thermal fluctuations of the writhe to the total free energy of supercoiling, addressed below. In Appendix C we address the second effect, the mechanical buckling instability of a circular (or superhelical) wire that occurs as the excess linking number is increased.

1. Writhe fluctuations are excess areas traced by the tangent

Up to an integer offset that may be set by continuity, the writhe is equal to the total area $\mathcal{A}$ on the unit sphere divided by 2π, which is swept out by the tangent vector $\hat{\mathbf{t}}$: $\mathrm{Wr}|_{\mathrm{mod}\,1} = \mathcal{A}/2\pi|_{\mathrm{mod}\,1}$. For small fluctuations around a superhelical structure, the quantity $\Delta\mathcal{A}$ is simply the excess area swept out by the tangent vector, where *excess area* refers to the area *between* the paths of $\hat{\mathbf{t}}$ and $\hat{\mathbf{t}}_0$ on the unit sphere.

The sign taken by $\Delta\mathcal{A}$ for fluctuations around regular helices follows some simple rules. First, for a right-handed solenoid, the reference tangent vector $\hat{\mathbf{t}}_0$ traces out a circle on the sphere. We choose the north pole or z axis so that this path is a line of latitude in the northern hemisphere. Now we see that the (smallest) region between the fluctuating path $\hat{\mathbf{t}}$ and the reference path $\hat{\mathbf{t}}_0$ may be divided up into patches that are to the north and to the south of this line of latitude. The areas of the regions south of $\hat{\mathbf{t}}_0$ are positive; the regions to the north are negative. For a left-handed solenoid, the signs are reversed since the writhe changes sign under parity due to its triple product.

For plectonemic superhelices, the reference tangent $\hat{\mathbf{t}}_0$ traces out two circles on the surface of the unit sphere, which mark two lines of latitude at equal levels in the northern and southern hemispheres. These circulate with opposite handedness around the north pole. Consider a right-handed plectoneme: the tangent circulates in a right-handed fashion around the north pole when it is in the northern hemisphere and it circulates in a left-handed fashion around the north pole when it is in the southern hemisphere. Again the areas between the paths of the reference tangent and the fluctuation tangent must be signed, the rule being that the more equatorial regions have a positive sign, the more polar regions are negative (a generalization of the above rule). Again, the sign conventions are reversed if a left-handed plectoneme is considered.

These rather cumbersome sign rules may be simply summarized by a simple formula, if we use (right-handed) polar coordinates Θ and Φ to describe the location of the tangent vector on the unit sphere, where the poles are defined as above, so that the reference tangent vectors sweep out lines of latitude (constant Θ), and the polar coordinates are referenced to the pole of the hemisphere containing $\hat{\mathbf{t}}_0$. Then,

$$\Delta\mathcal{A} = \int ds \frac{d\Phi}{ds}(\sin\gamma - \cos\Theta), \qquad \text{(B1)}$$

where $\sin\gamma$ is the superhelix angle defined above.

2. Writhe fluctuations are a subleading correction

Above we completely ignored the terms in the Hamiltonian having to do with the writhe fluctuations. Here we will consider these terms involving $\Delta\mathcal{A}$ further to show that this is a reasonable approach for large $X \equiv |C'\omega_0\sigma|$.

We need expressions for the polar angles of the tangent vector introduced above in terms of components of $\mathbf{u}$. We begin by noting that the polar angle is simply related to z component of the tangent: $\cos\Theta = t_z = \sin\gamma + \partial_s u_z$. This is an exact relation, so we only require $d\Phi/ds$ to linear order in $\mathbf{u}$ to obtain Gaussian $[O(u^2)]$ accuracy for $\Delta\mathcal{A}$.

Using space-fixed x and y coordinates we have

$$t_x + it_y = e^{\pm is/l}\{-\ell[\partial_s^2 u_\theta + a\partial_s^2 u_z + u_\theta/\ell^2] + i[1/(1+a^2)^{1/2} - a\partial_s u_z]\} + O(u^2), \quad \text{(B2)}$$

where the signs in the exponential are + for a right-handed superhelix and − for a left-handed one. The azimuthal angle is $\Phi = \arctan(t_y/t_x)$ and therefore

$$\frac{d\Phi}{ds} = \frac{t_x\partial_s t_y - t_y\partial_s t_x}{t_x^2 + t_y^2}, \quad \text{(B3)}$$

which can be worked out to be

$$\frac{d\Phi}{ds} = \frac{\pm 1}{\ell}[1 + (1+a^2)^{1/2}\left(\ell^2\partial_s^3 + \partial_s\right)u_\theta + a(1+a^2)^{1/2}\ell^2\partial_s^3 u_z + O(u^2)], \quad \text{(B4)}$$

where again the upper and lower signs are for right-handed and left-handed superhelices.

Finally, we obtain

$$\Delta\mathcal{A} = -\int ds \frac{d\Phi}{ds}\partial_s u_z \quad \text{(B5)}$$

$$= \pm(1+a^2)^{1/2}\int \frac{ds}{\ell}[\ell^2\partial_s^2 u_\theta \partial_s^2 u_z - \partial_s u_\theta \partial_s u_z + a\ell^2(\partial_s^2 u_z)^2] + O(u^3),$$

where terms linear in u have been integrated to zero and we have rearranged some of the derivatives in the quadratic terms. In terms of Fourier components,

$$\Delta\mathcal{A} = \pm\frac{1}{2}\int \frac{dk}{2\pi\ell^4} u_{ik}^* W_{ij} u_{jk} + O(u^3), \quad \text{(B6)}$$

where we have

$$W_{\theta\theta} = 0, W_{zz} = 2a(1+a^2)^{1/2}k^4, \quad \text{(B7)}$$
$$W_{\theta z} = W_{z\theta} = (1+a^2)^{1/2}k^2(k^2-1),$$

with k and a as in Appendix A and where upper and lower signs refer to right-handed and left-handed superhelices.

The quadratic portion of the fluctuation energy including the effects of writhe fluctuation is hence

$$\frac{\Delta E}{k_B T} = \frac{A}{2}\int \frac{dk}{2\pi\ell^5} u_i^* \left(E_{ij} \mp w W_{ij}\right) u_j + O(u^3), \quad \text{(B8)}$$

where we have the dimensionless constant

$$w = \frac{C\ell}{A}\left(\sigma\omega_0 - \frac{2\pi \mathrm{Wr}_0}{L}\right). \quad \text{(B9)}$$

The coupling w is expected to be positive for $\sigma > 0$ and negative for $\sigma < 0$ since the writhe is expected to only partially compensate the excess linking number. In combination with the fact that we expect right-handed solenoids and left-handed plectonemes for $\sigma > 0$ and the reverse for $\sigma < 0$, we see that W_{ij} in (B8) tends to soften the normal modes of solenoids and harden those of plectonemes.

The behavior of the constant w for large X superhelices is easily derived since we know that $\ell \approx C/X$ for both types of superhelices and $\sigma\omega_0 - 2\pi\mathrm{Wr}_0/L \approx X^{1/2}/C$ for the plectoneme and X/C for the solenoid. Thus $w \approx 1/X^{1/2}$ for the plectoneme and $w \approx 1$ for the solenoid. In the plectoneme case, this factor already acts to suppress the effect of the writhe fluctuations.

In addition to the factor w, the writhe fluctuation contribution to the free energy is further suppressed by the fact that W is less divergent than E at large k. Since W carries only k^4 terms, it cannot compete with the eigenvalue λ^+ of E, which has k^6 terms. However, it is not clear that λ_-, which has only k^4 terms, can dominate W. However, in the direction of the eigenvector $\mathbf{e}_- \propto -a\hat{\theta} + \hat{\mathbf{z}} + O(k^{-2})$, W actually has no k^4 contribution,

$$\mathbf{e}_-^T W \mathbf{e}_- = O(k^2). \quad \text{(B10)}$$

Since W does not alter the large-k dependence that generated the $-2/3$-law divergences in the confinement entropy, we expect no change of this result. Alternatively, the expectation value of the writhe fluctuation contribution to the free energy should be small compared to the bending free-energy fluctuation computed earlier.

We may calculate the expectation value of $\Delta\mathcal{A}$ to illustrate this explicitly:

$$\langle\Delta\mathcal{A}\rangle = L\int \frac{dk}{2\pi\ell^4}[a(1+a^2)^{1/2}k^4\langle u_{zk}^* u_{zk}\rangle + (1+a^2)^{1/2}k^2(k^2-1)\langle u_{\theta k}^* u_{zk}\rangle], \quad \text{(B11)}$$

where the expectation values are taken in the ensemble of Appendix A that results from the bending fluctuation energy. The divergences of the modes of the bending energy matrix (A7) are assumed to be cut off by the masses introduced to enforce the confinement constraint. Straightforward algebra yields

$$\langle\Delta A\rangle = \frac{L}{A}\int \frac{dk}{2\pi}\Bigg[a(1+a^2)^{1/2}k^4 \times \left(\frac{1}{1+a^2}\frac{1}{k^4} + \frac{3a^2}{(1+a^2)^2}\frac{1}{k^6} + \cdots\right) \quad \text{(B12)}$$

$$+(1+a^2)^{1/2}k^2[k^2-1]\left(\frac{-a}{1+a^2}\frac{1}{k^4}\right. \quad \text{(B13)}$$

$$\left. + \frac{-3a(1+2a^2)}{(1+a^2)^2}\frac{1}{k^6} + \cdots\right)\Bigg]. \quad \text{(B14)}$$

At this point the $O(1)$ terms all cancel, leaving a convergent integral. This occurs because of the subleading

high-k dependence of W discussed earlier. The result is

$$\langle \Delta \mathcal{A} \rangle = -\frac{L}{A} \int \frac{dk}{2\pi} \frac{2a}{(1+a^2)^{1/2} k^2} + \cdots \approx \frac{L}{A} \frac{a}{(1+a^2)^{1/2}} \frac{1}{m}, \quad \text{(B15)}$$

where the final integral is estimated using a cutoff k of largest mass m in the theory, which is $O(1)$ for the scaling solutions of Sec. IV D.

In the solenoid supercoil scaling limit, the writhe fluctuations are strongly suppressed since $a \approx X^{-1/2}$. We see that the two writhe fluctuation contributions to (22) from (19) are of order

$$C(\sigma\omega_0 - 2\pi \mathrm{Wr}_0/L) \langle \Delta \mathcal{A} \rangle \approx (L/A) X^{1/2} \quad \text{(B16)}$$

and

$$CL \langle \Delta \mathcal{A}/L \rangle^2 \approx CL/(A^2 X^2), \quad \text{(B17)}$$

which are small compared to the bending fluctuation free energy of order XL/C.

For the plectoneme, $a \approx X^{1/2}$ and we have a relatively large area fluctuation of order $\Delta \mathcal{A} \approx L/A$. The total writhe fluctuation contributions to the free energy are

$$C(\sigma\omega_0 - 2\pi \mathrm{Wr}_0/L) \langle \Delta \mathcal{A} \rangle \approx (L/A) X^{1/2} \quad \text{(B18)}$$

and

$$CL \langle \Delta \mathcal{A}/L \rangle^2 \approx CL/A^2, \quad \text{(B19)}$$

which are again much smaller than the bending fluctuation free energy of order XL/C.

Thus, in each case, the writhe fluctuations do not affect the scaling limit of the free energy. However, they are of great importance to the supercoil structure for $X \approx 1$ or near the random-coil to supercoil crossover. The formalism outlined here is a starting point for more detailed consideration of the effects of these fluctuations.

APPENDIX C: SUPERCOILING INSTABILITY OF A CIRCLE

How do our normal modes connect to the classic zero-temperature elastic studies of supercoiling instabilities [22–24]? The major result is that for an excess linking number $\Delta \mathrm{Lk} > \sqrt{3} A/C$ a circle is unstable and a transition occurs to a presumably supercoiled conformation. This zero-temperature transition linking number is independent of the length of the circle: we see that except for tiny rings of only a couple of persistence lengths, our fluctuation model shows that this instability is not important. The strong disordering effect of thermal fluctuations delays the formation of a plectonemic supercoil until $\Delta \mathrm{Lk} \approx L/C$ (note the L dependence of the thermally driven transition); below this threshold we expect a chirally biased random-coil conformation that has very little to do with the zero-temperature instability. However, it is useful to know how to connect to the zero-temperature regime.

Small fluctuations about a solenoidal superhelix with fixed average radius and pitch are described by the Gaussian energy

$$\frac{\Delta E}{k_B T} = \frac{A}{2} \int \frac{dk}{2\pi \ell^5} u^*_{ik} (E_{ij} - w W_{ij}) u_{jk}, \quad \text{(C1)}$$

where $w = (C\ell/A)(\sigma\omega_0 - 2\pi \mathrm{Wr}_0/L)$; for $|\sigma| > 0$ we see that w can drive an instability.

For a circle, we have $w = (C/A)\Delta \mathrm{Lk}$, $\ell = R$, and $P = 0$, leading to

$$E - wW = \begin{pmatrix} (k^2+1)(k^2-1)^2 & -wk^2(k^2-1) \\ -wk^2(k^2-1) & k^4 \end{pmatrix}. \quad \text{(C2)}$$

The low-energy eigenvalue is negative and fluctuations at wave number k are therefore unstable if $w^2 > k^2 + 1$ or if $|\Delta \mathrm{Lk}| > \sqrt{k^2+1} A/C$. The sign of the linking number does not affect the instability (sign reversal of $\Delta \mathrm{Lk}$ is a symmetry) and the amplitude has the same scaling with A and C. For a circle, the periodic boundary condition indicates that only $k = 0, \pm 1, \pm 2, \pm 3, \ldots$ are allowed. The first k for which the low-lying mode is not a symmetry operation is $k = \pm 2$ (the low-energy mode with $k = 0$ generates translation along z; those with $k = \pm 1$ generate translation in the x-y plane), indicating instability beyond $\Delta \mathrm{Lk} > \sqrt{5} A/C$.

So where is the $\sqrt{3}$ [23,24]? Our helix calculation is not quite the right thing to use for the circle-instability calculation because we have used the fixed-average-radius ensemble, omitting the final term of the curvature expansion (A2). The u_r contribution from (A3) after application of (A5) slightly modifies the bending energy matrix

$$E_{\theta\theta} = k^2(k^2-1)^2, \quad E_{zz} = k^2(k^2-1) + a^2 k^4 (k^2+5), \quad \text{(C3)}$$

$$E_{\theta z} = E_{z\theta} = a k^2 (k^2+2)(k^2-1). \quad \text{(C4)}$$

Fluctuations of a circle ($a = 0$) are described by the energy

$$E - wW = k^2(k^2-1) \begin{pmatrix} k^2-1 & -w \\ -w & 1 \end{pmatrix}. \quad \text{(C5)}$$

Now the low-energy mode becomes negative in energy for $|w| > k^2 - 1$, which for $k = 2$ is the condition $|\Delta \mathrm{Lk}| > \sqrt{3} A/C$. The instability occurs for slightly less excess linking because we have removed the constraint that the radius be fixed [23,24].

APPENDIX D: STATISTICS OF LONG UNSUPERCOILED DNA MOLECULES

Here we review [63] why unsupercoiled DNA molecules shorter than 100 kbp have Gaussian statistics. Because DNA is stiff, each statistical monomer (each 300 bp segment) is a thin rod. The excluded volume between two statistical monomers is a small fraction of the cube of the

monomer length. The resulting weak self-avoidance has no effect on the statistics of chains of less than 100 kbp.

The excess free energy per particle due to self-avoidance effects in a gas of hard rods of length b and diameter D at a concentration ϕ is [62]

$$\frac{F_{SA}}{k_BT} = \frac{\pi}{4} b^2 D\phi + O(\phi^2). \quad \text{(D1)}$$

The quantity b^2D is the volume excluded from a rod's phase space due to one other rod; for each state where the rods are within b of one another (a volume b^3) a fraction D/b of the orientations is excluded (the solid angle subtended by the rod at the origin is of order D/b at a distance of order b). We can use this result to estimate the effects of self-avoidance on polymers composed of rod-like segments, such as DNA.

The standard Flory model [64] can be used to determine the coil radius R_g; the free energy of a chain is a sum of elastic and self-avoidance contributions

$$\frac{F}{k_BT} = \frac{R_g^2}{Nb^2} + \frac{b^2DN^2}{R_g^3}, \quad \text{(D2)}$$

where b is now the segment size, N is the number of segments along the chain, and we have used (D1) to estimate the excluded-volume interaction. However, if the last term is smaller than unity for the Gaussian size $R_0 \approx bN^{1/2}$, i.e., if $N < b^2/D^2$, there will be no appreciable swelling. For $N > b^2/D^2$ the coil size is $R_g \approx (b^4D)^{1/5}N^{3/5}$.

For unsupercoiled DNA we take the segment size to be $b = 2A = 100$ nm (the end-to-end radius of a Gaussian persistent chain is $R_0 = \sqrt{2AL}$), $N = L/2A$, and $D = 4$ nm (an appropriate hard-core diameter at 200 mM NaCl). Thus DNA is swollen by self-avoidance for $L > 8A^3/D^2 \approx 6\times10^4$ nm $\approx 2\times10^5$ bp. Nearly the same estimate is obtained from the asymptotic series for chain radius using the criterion that the dimensionless expansion parameter [64] $z = (3/2\pi)^{3/2}\pi N^{1/2}D/2b$ is 1/2.

The upshot is that self-avoidance is important only for DNA molecules substantially longer than plasmids, cosmids, and domain sizes typically encountered in either prokaryotic or eukaryotic genomes. Gaussian statistics should therefore generally be used to describe unsupercoiled DNA molecules.

[1] J. Vinograd J. Lebowitz, R. Radloff, R. Watson, and P. Lapis, Proc. Natl. Acad. Sci. U.S.A. **53**, 1104 (1965).
[2] A. Worcel and E. Burgi, J. Mol. Biol. **71**, 127 (1972).
[3] C. Benyajati and A. Worcel, Cell **9**, 393 (1976).
[4] D. A. Jackson, P. Dickinson, and P. R. Cook, EMBO J. **9**, 567 (1990).
[5] A. P. Wolffe, *Chromatin* (Academic, New York, 1993).
[6] L. A. Freeman and W. T. Garrard, Crit. Rev. Euk. Gene Exp. **2**, 165 (1992).
[7] F. B. Fuller, Proc. Natl. Acad. Sci. U.S.A. **68**, 815 (1971).
[8] T. C. Boles, J. H. White, and N. R. Cozzarelli, J. Mol. Biol. **213**, 931 (1990).
[9] J. F. Marko and E. D. Siggia, Science **265**, 506 (1994).
[10] O. G. Berg, Biopolymers **23**, 1869 (1984).
[11] C. N. Parker and S. E. Halford, Cell **66**, 781 (1991).
[12] P. G. de Gennes, *Scaling Concepts in Polymer Physics* (Cornell University Press, Ithaca, 1990).
[13] For a more complete discussion of DNA structure and function see J. Darnell, H. Lodish, and D. Baltimore, *Molecular Cell Biology* (Scientific American Books, New York, 1990), pp. 68–72.
[14] Measurement of A by a variety of groups yields values close to 50 nm: P. J. Hagerman, Annu. Rev. Biophys. Biophys. Chem. **17**, 265 (1988). In this paper we take $A = 50$ nm.
[15] Values for C determined experimentally range from 40 to 100 nm: W. H. Taylor and P. J. Hagerman, J. Mol. Biol. **212**, 363 (1990); D. M. Crothers, J. Drak, J. D. Kahn, and S. D. Levene, Methods Enzymol. **212**, 3 (1992). We take $C = 75$ nm as in Ref. [26].
[16] J. C. Wang, J. Biol. Chem. **266**, 6659 (1991); M. B. Schmid and J. A. Sawitzke, Bioessays **15**, 445 (1993).
[17] S. A. Wasserman and N. R. Cozzarelli, J. Bio. Chem. **266**, 20567 (1991).
[18] W. R. Bauer, Ann. Rev. Biophys. Bioeng. **7**, 287 (1978).
[19] M. B. Schmid, Trends Biochem. Sci. **13**, 131 (1988).
[20] An excellent review of supercoiling is by N. R. Cozzarelli, T. C. Boles, and J. White, in *DNA Topology and its Biological Effects*, edited by N. R. Cozzarelli and J. C. Wang (Cold Spring Harbor Laboratory, Cold Spring Harbor, NY, 1990), Chap. 4.
[21] M. Adrian, B. ten Heggeler-Bordier, W. Wahli, A. Z. Stasiak, A. Stasiak, and J. Dubochet, EMBO J. **13**, 4551 (1990); J. Bednar, P. Furrer, A. Stasiak, J. Dubochet, E. H. Egelman, and A. D. Bates, J. Mol. Biol. **235**, 825 (1994); J. Dubochet, J. Bednar, P. Furrer, and A. Stasiak, in *Structural Biology: The State of the Art, Proceedings of the Eighth Conversation*, edited by R. H. Sarma and M. H. Sarma (Adenine, Schenectady, 1994).
[22] M. Le Bret, Biopolymers **18**, 1709 (1979); C. J. Benham, *ibid.* **22**, 2477 (1983); M. Le Bret, *ibid.* **23**, 1835 (1984); F. Tanaka and H. Takahashi, J. Chem. Phys. **83**, 6017 (1985).
[23] C. J. Benham, Phys. Rev. A **39**, 2582 (1989).
[24] E. Guitter and S. Leibler, Europhys. Lett. **17**, 643 (1992).
[25] K. V. Klenin, A. V. Vologodskii, V. V. Anmshelevich, A. M. Dykhne, and M. D. Frank-Kamenetskii, J. Mol. Biol. **217**, 413 (1991).
[26] A. V. Vologodskii, S. D. Levene, K. V. Klenin, M. Frank-Kamenetskii, and N. R. Cozzarelli, J. Mol. Biol. **227**, 1224 (1992).
[27] A. V. Vologodskii and N. R. Cozzarelli, Annu. Rev. Biophys. Biomol. Struct. **23**, 609 (1994).
[28] A. V. Vologodskii and M. D. Frank-Kamenetskii, Methods Enzymol. **211**, 468 (1992); A. V. Vologodskii and N. R. Cozzarelli, Curr. Opin. Struct. Biol. **4**, 372 (1994).
[29] K. V. Klenin, M. D. Frank-Kamenetskii, and J. Langowski, Biophys. J. **68**, 81 (1995).
[30] D. M. Crothers, T. E. Haran, and J. G. Nadeau, J. Biol. Chem. **265**, 7093 (1990); J. D. Kahn, E. Yun, and D. C. Crothers, Nature **368**, 163 (1994).
[31] J. F. Marko and E. D. Siggia, Macromolecules **27**, 981

(1994).
[32] The Kuhn statistical segment length for this model is $b = 2A$. This is obtained by computing the average squared end-to-end distance for a phantom linear chain of length L and setting it equal to Lb, the corresponding result for a random walk of L/b steps each of length b. See M. Doi and S. F. Edwards, *The Theory of Polymer Dynamics* (Oxford University Press, New York, 1984), Sec. 8.8.
[33] J. A. Schellman and D. Stigter, Biopolymers **16**, 1415 (1977); D. Stigter, *ibid.* **16**, 1435 (1977).
[34] R. Podgornik and V. A. Parsegian, Macromolecules **23**, 2265 (1990).
[35] D. C. Rau and V. A. Parsegian, Biophys. J. **61**, 260 (1992); **61**, 246 (1992); S. Leikin, D. C. Rau, and V. A. Parsegian, Phys. Rev. A **44**, 5272 (1991).
[36] The effective charge ν is set by matching (2) to the solution of the Poisson-Boltzmann equation for a charged cylinder in an ionic solution, in the regime $r \gg \lambda_D$, where it reduces to the Debye-Huckel equation. Consequently, ν is not simply related to the structural charges ($\approx 6e$/nm) on DNA. For details see Ref. [33].
[37] G. Calagareau, Rev. Math. Pure Appl. **4**, 58 (1959); Czech. Math. J. **4** 588 (1961).
[38] J. H. White, Am. J. Math. **91**, 693 (1969).
[39] F. B. Fuller, Proc. Natl. Acad. Sci. U.S.A. **75**, 3557 (1978).
[40] J. H. White and W. R. Bauer, J. Mol. Biol. **189** 329, (1986).
[41] In this paper, τ is unsigned and always positive. For left-handed helices, the Frenet-Seret torsion is taken to be negative: we keep track of this sign explicitly.
[42] N. G. Hunt and J. E. Hearst, J. Chem. Phys. **95**, 9329 (1991).
[43] T. Schlick and W. K. Olson, J. Mol. Biol. **223**, 1089 (1992).
[44] K. V. Klenin, A. V. Vologodskii, V. V. Anshelevich, V. Yu. Klishko, A. M. Dkyhne, and M. D. Frank-Kamenetskii, J. Biomol. Struct. Dyn. **6**, 707 (1989); see also S. D. Levene and D. M. Crothers, J. Mol. Biol. **189**, 73 (1986); J. Shimada and H. Yamakawa, Biopolymers **27**, 657 (1988).
[45] R. E. Depew and J. C. Wang, Proc. Natl. Acad. Sci. U.S.A. **11**, 4275 (1975); D. E. Pulleyblank, M. Shure, D. Tang, J. Vinograd, and H.-P. Vosberg, *ibid.* **11**, 4280 (1975).
[46] This estimate of C is quite sensitive to the precise values of the well-known parameters ω_0, A, and α and this formula might provide a superior method for the measurement of C. Closely related methods have used computer simulation data to estimate A and C: see M. D. Frank-Kamenetskii, A. V. Lukashin, V. V. Anshelevich, and A. A. Vologodskii, J. Biomol. Struct. Dyn. **2**, 1005 (1989); A. V. Vologodskii, V. V. Anshelevich, A. V. Lukahin, and M. D. Frank-Kamenetskii, Nature **280**, 294 (1979).
[47] Stacked fluctuating membranes interact via a power-law interaction because their fluctuation entropy is reduced as they are pushed together. See W. Helfrich, Z. Naturforsch. Teil A **33**, 305 (1978); S. Leibler, in *Jerusalem Winter School for Theoretical Physics, Vol. 5: Statistical Mechanics of Membranes and Surfaces*, edited by D. Nelson, T. Piran, and S. Weinberg (World Scientific, Teaneck, NJ, 1989), pp. 81 and 82.
[48] W. Helfrich and W. Harbich, Chem. Scr. **25**, 32 (1985).
[49] T. Odijk, Macromolecules **17**, 502 (1984).
[50] L. D. Landau and E. M. Lifshitz, *Statistical Physics* (Pergamon, New York, 1978), Sec. 152.
[51] S. Y. Shaw and J. C. Wang, Science **260**, 533 (1993); V. V. Rybenkov, N. R. Cozzarelli, and A. V. Vologodskii, Proc. Natl. Acad. Sci. U.S.A. **90**, 5307 (1993).
[52] B. Zimm and W. H. Stockmayer, J. Chem. Phys. **17**, 1301 (1949).
[53] M. Doaud and J. F. Joanny, J. Phys. (Paris) **42**, 1359 (1981).
[54] H. A. Benjamin and N. R. Cozzarelli, Proc. R. A. Welch Found. Conf. Chem. Res. **29**, 107 (1986).
[55] S. J. Spengler, A. Stasiak, and N. R. Cozzarelli, Cell **42**, 325 (1985).
[56] M. Doi, Chem. Phys. **11**, 115 (1975).
[57] S. B. Smith, L. Finzi, and C. Bustamante, Science **258**, 1122 (1992).
[58] M. Fixman and J. Kovac, J. Chem. Phys. **58**, 1564 (1973).
[59] C. Bustamante, J. F. Marko, E. D. Siggia, and S. B. Smith, Science **265**, 1599 (1994); A. Vologodskii, Macromolecules **27**, 5623 (1994); J. F. Marko and E. D. Siggia, Macromolecules (to be published).
[60] L. F. Liu and J. C. Wang, Proc. Natl. Acad. Sci. U.S.A. **84**, 7024 (1987); P. Droge, Bioessays **16**, 91 (1994).
[61] A. V. Vologodskii (private communication). For experiments on catenated DNA molecules, see Ref. [55]; D. E. Adams, E. M. Shekhtman, E. L. Zechiedrich, M. B. Schmidt, and N. R. Cozzarelli, Cell **71**, 277 (1992).
[62] L. Onsager, Ann. N. Y. Acad. Sci. **51**, 627 (1949).
[63] T. Odijk, Biopolymers **18**, 3111 (1979); G. Manning, *ibid.* **20**, 1751 (1981); C. B. Post, *ibid.* **22**, 1087 (1983).
[64] M. Doi and S. F. Edwards, *The Theory of Polymer Dynamics* (Ref. [32]), Sec. 2.5.